Electronic Supplementary Information

Practice of Function-Oriented Synthesis: High-Efficiency CO_2 Conversion and Knoevenagel Condensation by Two Novel In_3-based MOFs with High-Density Active Sites under Mild Conditions

*Junyi Qiao, Borong Zhang, Lirong Zhang, and Yunling Liu**

State Key Laboratory of Inorganic Synthesis and Preparative Chemistry, College of Chemistry, Jilin University, Changchun 130012, P. R. China. Email: yunling@jlu.edu.cn

Table of Contents:

S1. Synthesis of H_3BTCTBA ligand.

Synthesis of 4,4',4''-[1,3,5-benzenetriyltris(carbonylimino)]trisbenzoic acid (H_3BTCTBA)

H_3BTCTBA ligand was synthesized according to a literature with slight modifications.[1] 4-aminobenzoic acid (6.0 g, 23.4 mmol) and K_2CO_3 (13.0 g, 92 mmol) were dissolved in 120 mL dry acetone and stirred under N_2 atmosphere at room temperature for 15 min. A solution of 1,3,5-benzenetricarbonyltrichloride (12.6 g, 92 mmol) in 60 mL acetone was added slowly in 10 min. The mixture was stirred at 65 °C overnight. After cooling, the resultant precipitate was separated by filtration, washed with water (200 mL) and acetone (30 mL), and then dried at 60 °C under vacuum to obtain H_3BTCTBA as white solid.

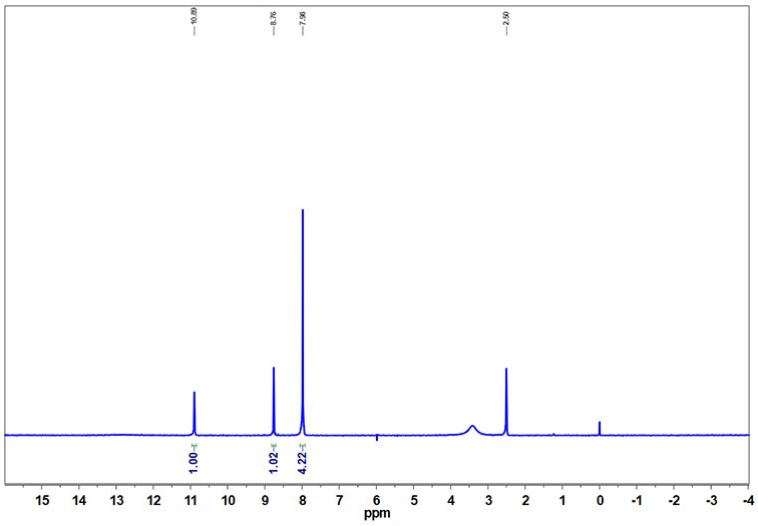

Fig. S1. ^{1}H NMR spectrum of H_3BTCTBA.

S2. Crystallographic data and structures of JLU-MOF116 and 117.

Table S1. Crystal data and structure refinement of **JLU-MOF116**.

Compound	**JLU-MOF116**
Formula	$C_{46}H_{26}In_3N_4O_{20}$
Formula Weight	1299.17
Temperature (K)	293(2)
Crystal System	Tetragonal
Space Group	$P4_2/mnm$
a (Å)	30.241(4)
b (Å)	30.241(4)
c (Å)	18.297(4)
α (°)	90
β (°)	90
γ (°)	90
V (Å^3)	16734(6)
Z, ρ_{calc} (g/cm^3)	4, 0.516
μ (mm^{-1})	0.434
F(000)	2548.0
2θ Range for Data Collection (°)	5.984 to 54.962
Reflections Collected	153985
Independent Reflections	10112 [R_{int} = 0.1321, R_{sigma} = 0.0526]
Data/Restraints/Parameters	10112/275/254
Goodness-of-fit on F^2	1.016
Final R Indexes [I ≥ 2σ (I)]	$R_1{}^a$ = 0.0542, $wR_2{}^b$ = 0.1543
Final R Indexes [all data]	$R_1{}^a$ = 0.0779, $wR_2{}^b$ = 0.1648

^{a} $R_1 = \Sigma||F_o| - |F_c||/\Sigma|F_o|$, ^{b} $wR_2 = [\Sigma w(|F_o|^2 - |F_c|^2)/\Sigma|w(F_o^2)^2|]^{1/2}$

Table S2. Crystal data and structure refinement of **JLU-MOF117**.

Compound	**JLU-MOF117**
Formula	$C_{60}H_{30}In_3N_6O_{22}$
Formula Weight	1531.36
Temperature (K)	302.16
Crystal System	Orthorhombic
Space Group	*Imma*
a (Å)	20.1206(4)
b (Å)	28.9071(7)
c (Å)	29.2586(7)
α (°)	90
β (°)	90
γ (°)	90
V (Å^3)	17017.6(7)
Z, ρ_{calc} (g/cm^3)	4, 0.598
μ (mm^{-1})	0.433
F(000)	3020.0
2θ Range for Data Collection (°)	4.508 to 50.700
Reflections Collected	33311
Independent Reflections	8133 [R_{int} = 0.0851, R_{sigma} = 0.0989]
Data/Restraints/Parameters	8133/20/263
Goodness-of-fit on F^2	0.947
Final R Indexes [I ≥ 2σ (I)]	$R_1{}^a$ = 0.0411, $wR_2{}^b$ = 0.1065
Final R Indexes [all data]	$R_1{}^a$ = 0.0602, $wR_2{}^b$ = 0.1132

^{a} $R_1 = \Sigma||F_o| - |F_c||/\Sigma|F_o|$, ^{b} $wR_2 = [\Sigma w(|F_o|^2 - |F_c|^2)/\Sigma|w(F_o^2)^2|]^{1/2}$

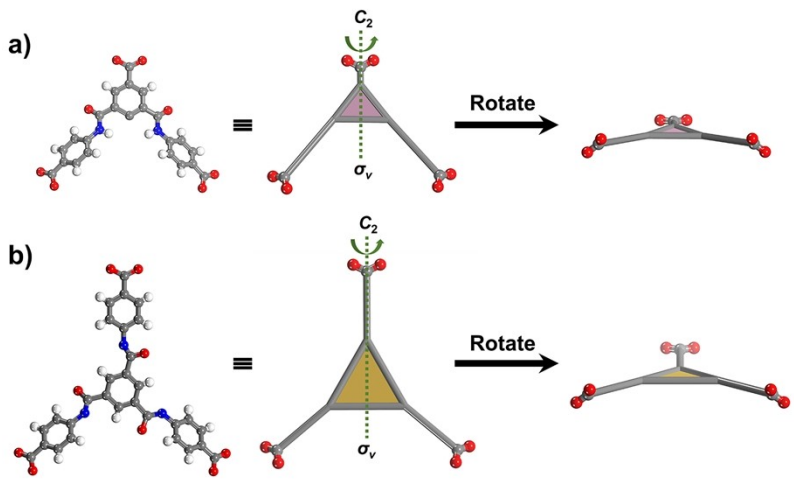

Fig. S2. Molecular symmetries of BCPACBA and BTCTBA.

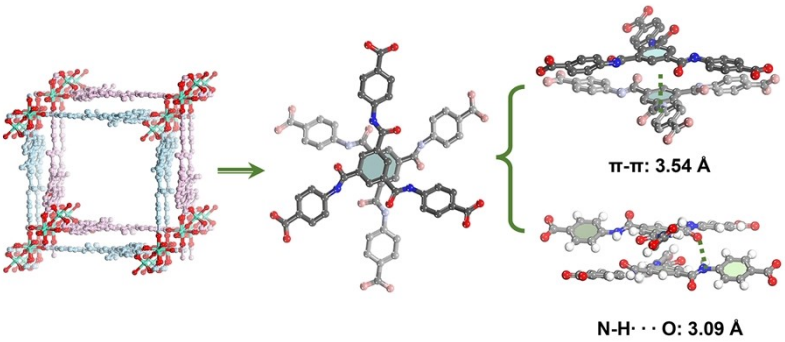

Fig. S3. The 2-fold interpenetration framework of **JLU-MOF117** showing N-H····O hydrogen-bond interactions and π-π interactions between the two adjacent BTCTBA ligands.

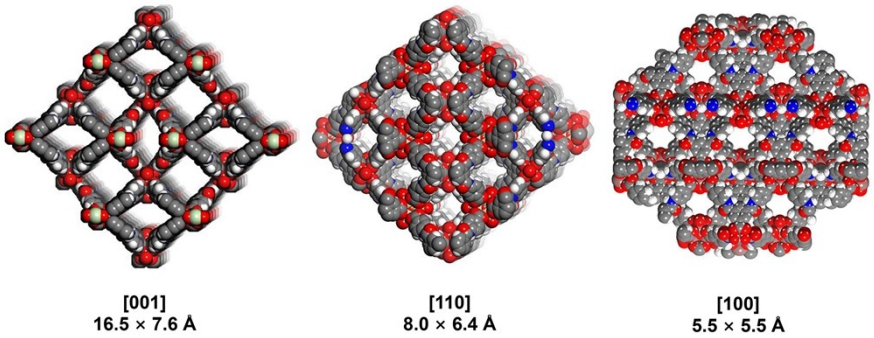

Fig. S4. CPK models of **JLU-MOF116** framework along the [001], [110], and [100] directions.

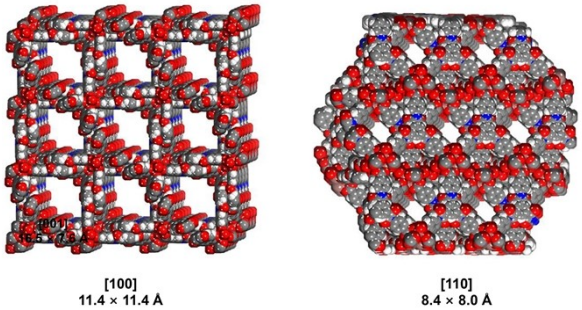

Fig. S5. CPK models of **JLU-MOF117** framework along the [100] and [110] directions.

S3. PXRD patterns, TGA analyses and N_2 sorption isotherms of JLU-MOF116 and 117.

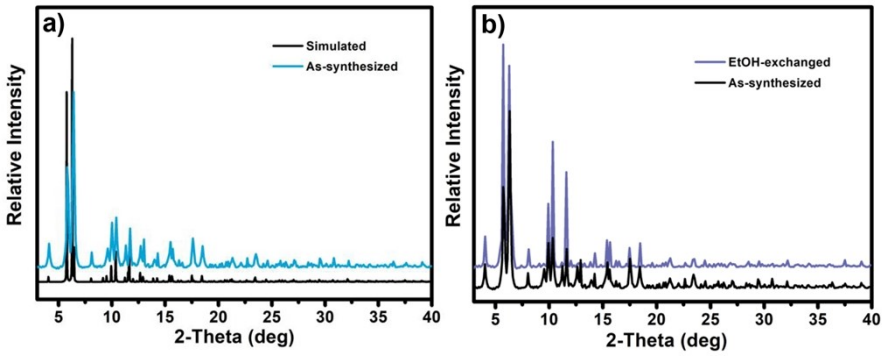

Fig. S6. PXRD patterns of a) simulated, as-synthesized, and b) EtOH-exchanged **JLU-MOF116**.

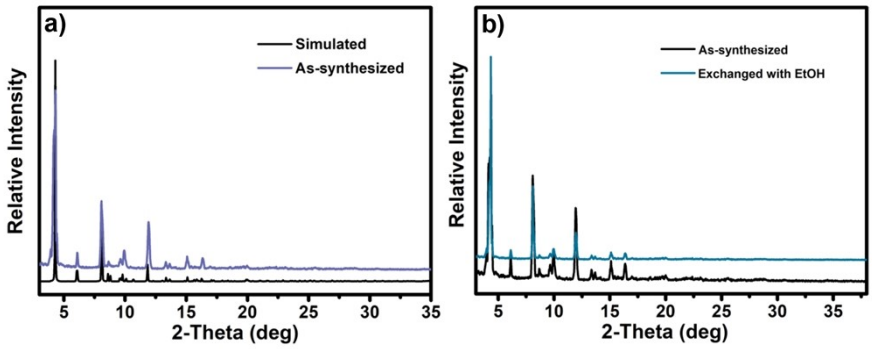

Fig. S7. PXRD patterns of a) simulated, as-synthesized, and b) EtOH-exchanged **JLU-MOF117**.

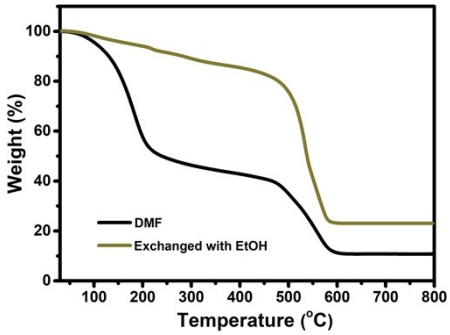

Fig. S8. TGA curves of the as-synthesized and ethanol-exchanged **JLU-MOF116**.

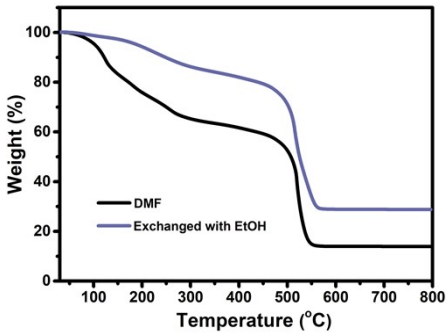

Fig. S9. TGA curves of the as-synthesized and ethanol-exchanged **JLU-MOF117**.

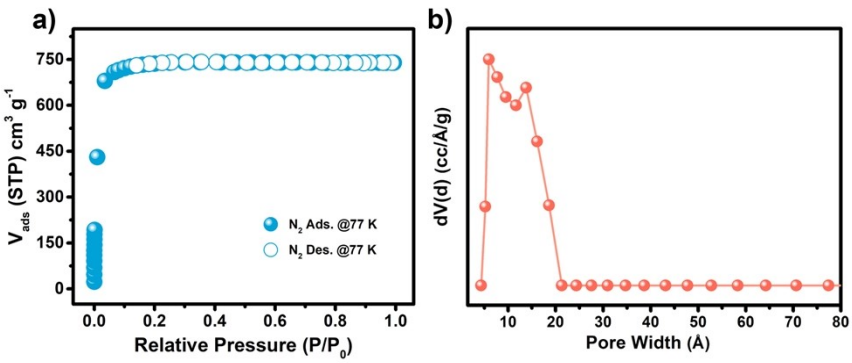

Fig. S10. a) N_2 adsorption-desorption isotherm and b) pore size distribution of **JLU-MOF116**.

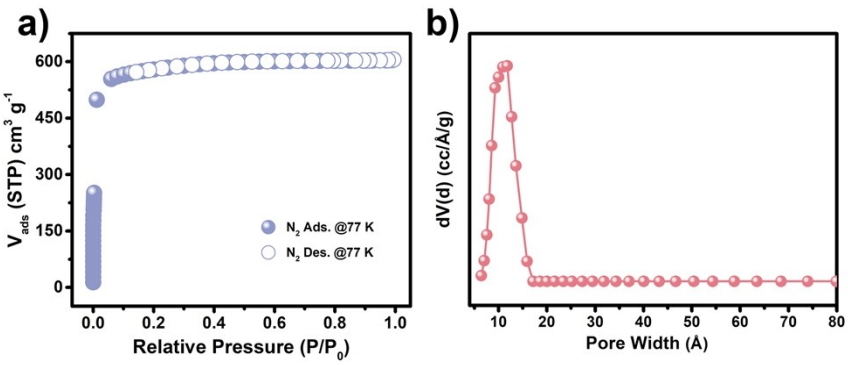

Fig. S11. a) N_2 adsorption-desorption isotherm and b) pore size distribution of **JLU-MOF117**.

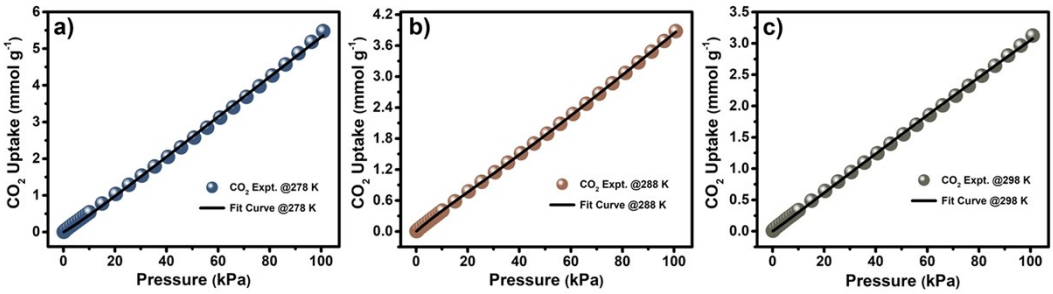

a_1	1.93249
a_2	77.59192
b_1	3.89927×10^{-4}
b_2	4.8525×10^{-4}
c_1	0.94911
c_2	1.08761
R-square	0.9993

a_1	39.76144
a_2	0.62537
b_1	2.15319×10^{-4}
b_2	0.05562
c_1	0.94911
c_2	1.00096
R-square	0.9999

a_1	33.18129
a_2	5.39567
b_1	8.37668×10^{-4}
b_2	1.68266×10^{-4}
c_1	1.01520
c_2	1.28242
R-square	0.9995

Fig. S12. Fitting curves and parameters of CO_2 adsorption isotherms of **JLU-MOF116** at a) 278, b) 288, and c) 298 K.

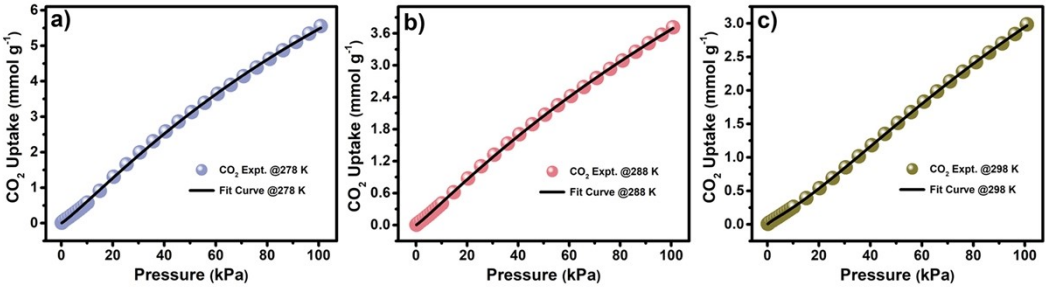

a_1	0.20717
a_2	15.79663
b_1	0.01000
b_2	0.00296
c_1	1.00000
c_2	1.12006
R-square	0.9998

a_1	1.7981
a_2	15.03825
b_1	0.0069
b_2	0.0015
c_1	1.12525
c_2	1.08028
R-square	0.9999

a_1	8.67867
a_2	0.08478
b_1	9.69725×10^{-4}
b_2	0.37933
c_1	1.03455
c_2	1.03455
R-square	0.9999

Fig. S13. Fitting curves and parameters of CO_2 adsorption isotherms of **JLU-MOF117** at a) 278, b) 288, and c) 298 K.

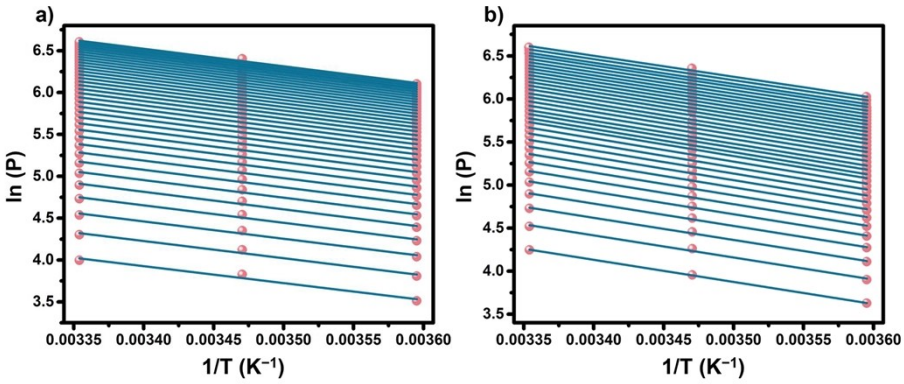

Fig. S14. The isosters of Q_{st} values for a) **JLU-MOF116** and b) **JLU-MOF117**.

S4. CO_2 conversions with epoxides catalyzed by JLU-MOF116 and JLU-MOF117.

Table S3. Comparisons of volumetric densities of amide groups in JLU-MOF116, 117, and other amide-based MOF materials.

Compound	Volumetric density of amide group (mol L^{-1})	Ref.
3W-ROD-1	2.5	2
sph-MOF-1	2.4	3
JLU-MOF117	2.4	This work
M_2(carboxylate)$_4$	2.1	4
JLU-MOF116	1.6	This Work
DUT-32	0.9	5

Table S4. The investigation of optimal conditions for CO_2 conversion by **JLU-MOF116** and **JLU-MOF117**.

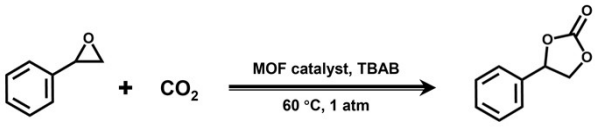

Entry [a]	JLU-MOF116				Entry [a]	JLU-MOF117			
	Cat. (mol%)	TBAB (mol%)	Time (h)	Yield (%)		Cat. (mol%)	TBAB (mol%)	Time (h)	Yield (%)
1	0.075	5	8	59	14	0.05	5	6	38
2	0.15	5	8	> 99	15	0.1	5	6	94
3	0.3	5	8	> 99	16	0.2	5	6	97
4	0.15	2	8	95	17	0.1	2	6	86
5	0.15	8	8	> 99	18	0.1	8	6	> 99
6	0.15	5	1	51	19	0.1	5	1	47
7	0.15	5	2	69	20	0.1	5	2	59
8	0.15	5	3	91	21	0.1	5	3	72
9	0.15	5	4	96	22	0.1	5	4	86
10	0.15	5	5	97	23	0.1	5	5	92
11	0.15	5	6	99	24	0.1	5	8	99
12	None	5	6	32	25	None	5	6	32
13 [b]	0.15	5	6	41	26 [b]	0.15	5	6	39

Reaction conditions: [a] Activated MOF catalysts, styrene oxide (10 mmol) and 1 atm CO_2 pressure. [b] As-synthesized MOF catalysts.

In order to determine the optimal reaction condition, a sequence of **JLU-MOF116**-catalyzed CO_2 conversion reactions with styrene oxide was performed at 60 °C and 1 atm CO_2 pressure. The amount of MOF catalyst was first explored within a prolonged reaction time and an appropriate TBAB amount of 5 mol%. CO_2 conversion with styrene oxide catalyzed by 0.075 mol% **JLU-MOF116** resulted in only 59% yield while gained nearly 100% yields by 0.15 and 0.3 mol% catalysts (Table S4, Entry 1-3). Accordingly, the appropriate catalyst amount was determined as 0.15 mol%. As an efficient nucleophile, the amount of TBAB co-catalyst also has an impact on CO_2 conversion. The yield was 95% and 99%, when 2 mol% and 5 mol% TBAB engaged in the reaction, respectively (Table S4, Entry 4 and 11). Thereby, the amount of TBAB was determined as 5 mol%. The optimal catalyst amounts were investigated in the same manner to be 0.1 mol% **JLU-MOF117** and 5 mol% TBAB (Table S4, Entry 15-19), which is also easy for comparison with **JLU-MOF116**. The kinetic curves of the CO_2 conversion reactions by **JLU-MOF116** and **117** were further investigated. The CO_2 conversions have already gained 51% and 47% yields for **JLU-MOF116** and **117** within the initial 1 h, respectively, reached up to 97% and 94% yields within the next 4 hours for **JLU-MOF116** and 5 hours for **JLU-MOF117**, respectively, and achieved equilibriums thereafter (Table S4, Entry 6-11, 20-25).

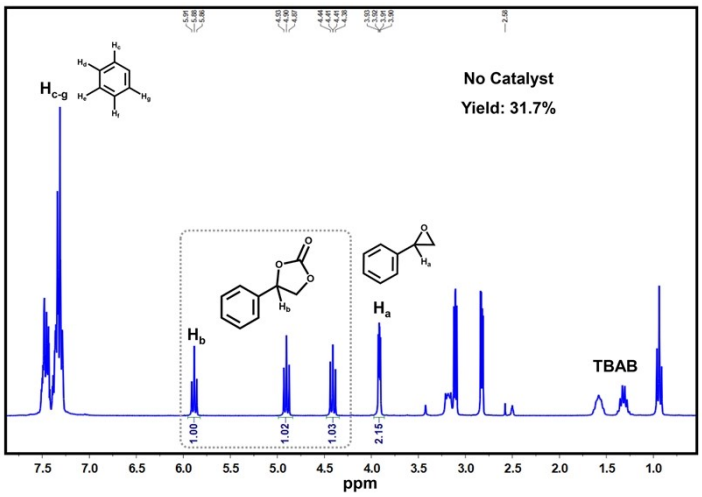

Fig. S15. ^{1}H NMR spectrum of CO_2 conversion with styrene oxide without MOF catalyst.

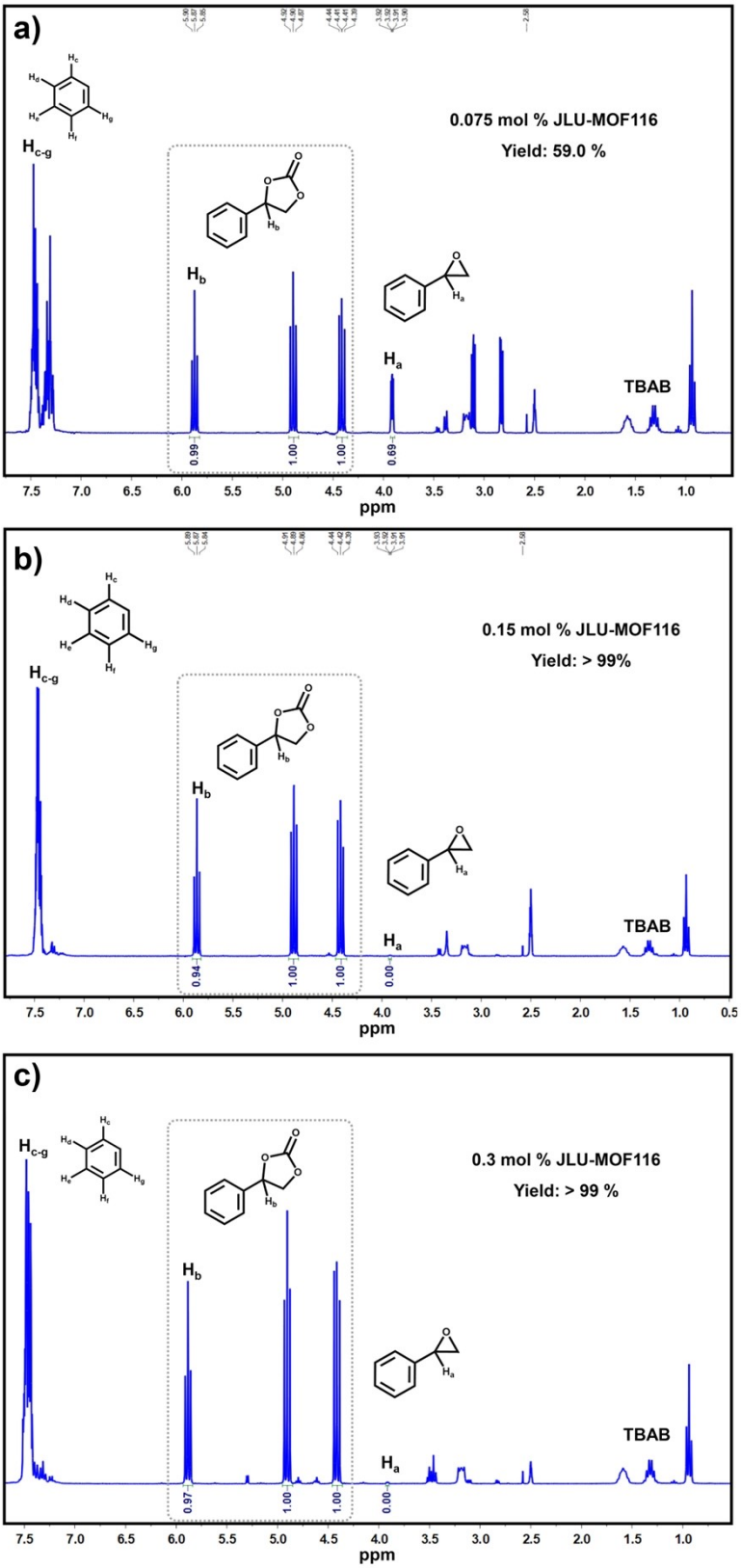

Fig. S16. ^{1}H NMR spectra of CO_2 conversion catalyzed by a) 0.075 mol%, b) 0.15 mol%, and c) 0.3 mol% **JLU-MOF116**.

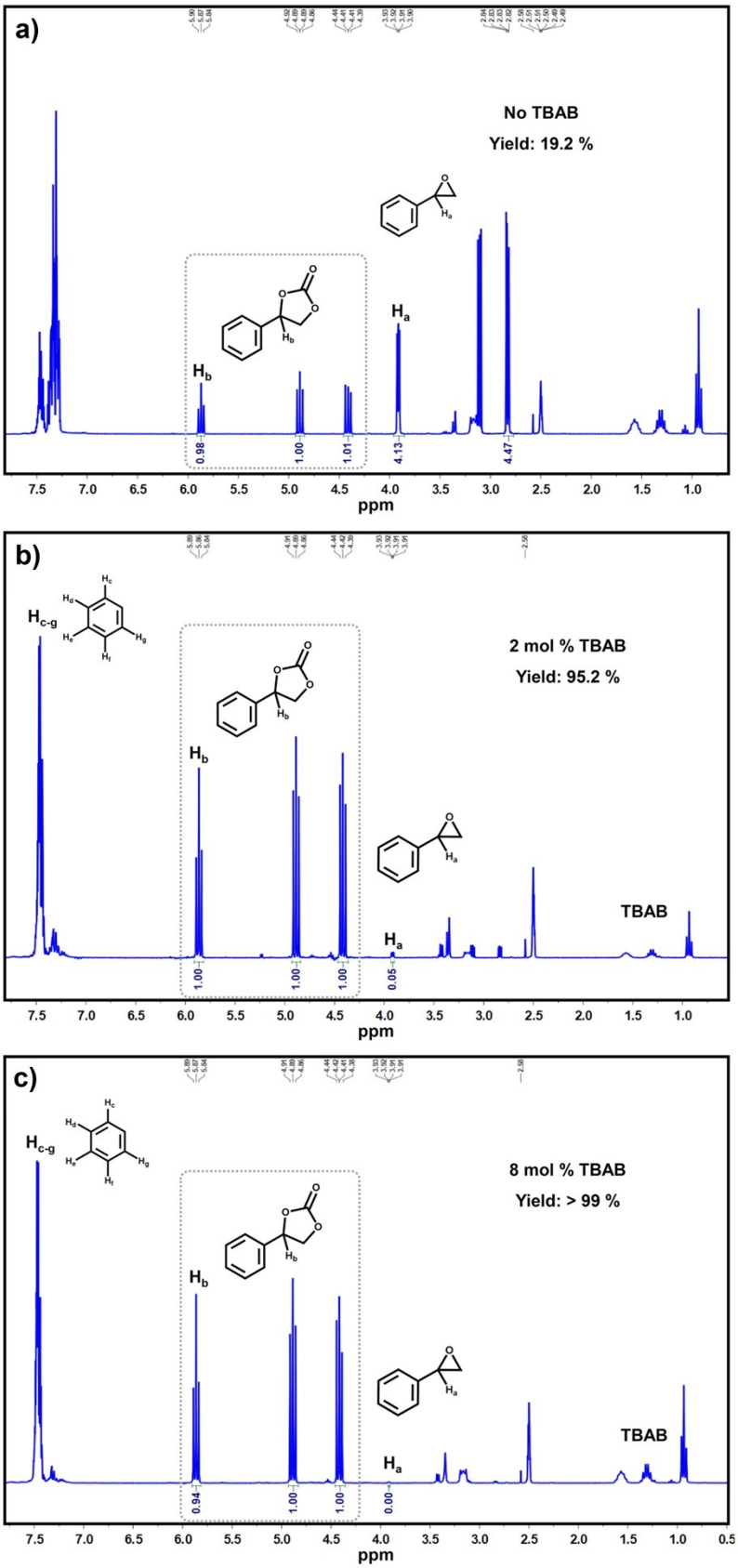

Fig. S17. ^{1}H NMR spectra of CO_2 conversion catalyzed by a) 0, b) 2 mol%, and c) 8 mol% TBAB and **JLU-MOF116**.

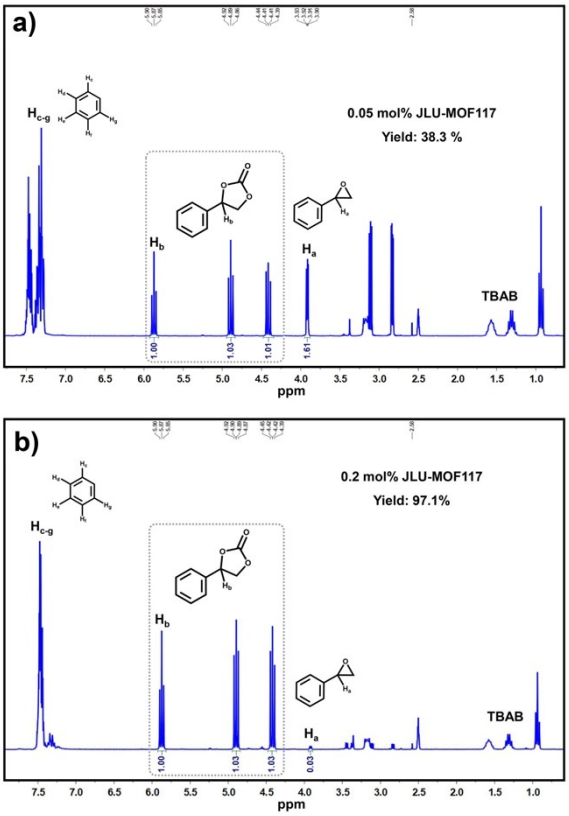

Fig. S18. ^{1}H NMR spectra of CO_2 conversion catalyzed by a) 0.05 mol% and b) 0.2 mol% **JLU-MOF117**.

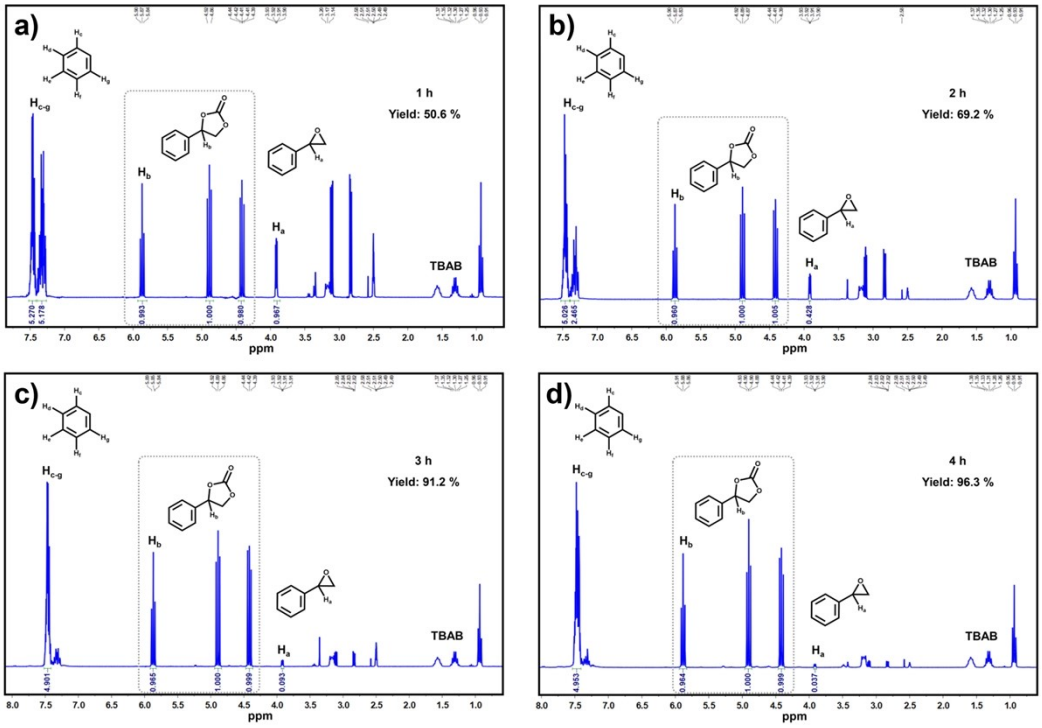

Fig. S19. ^{1}H NMR spectra of CO_2 conversion catalyzed by **JLU-MOF116** within a) 1 h, b) 2 h, c) 3 h, and d) 4 h.

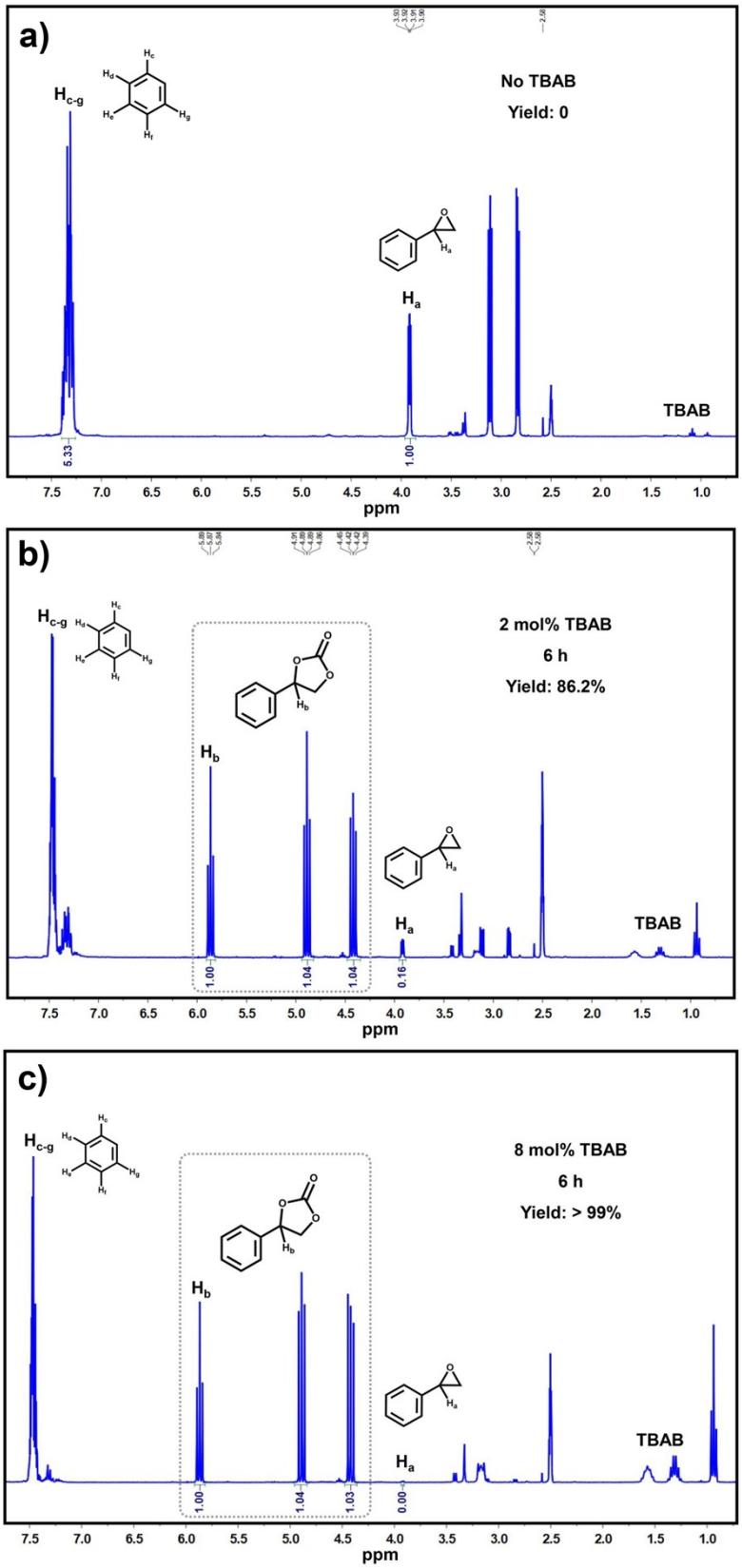

Fig. S20. ^{1}H NMR spectra of CO_2 conversion catalyzed by a) 0, b) 2 mol%, and c) 8 mol% TBAB and **JLU-MOF117**.

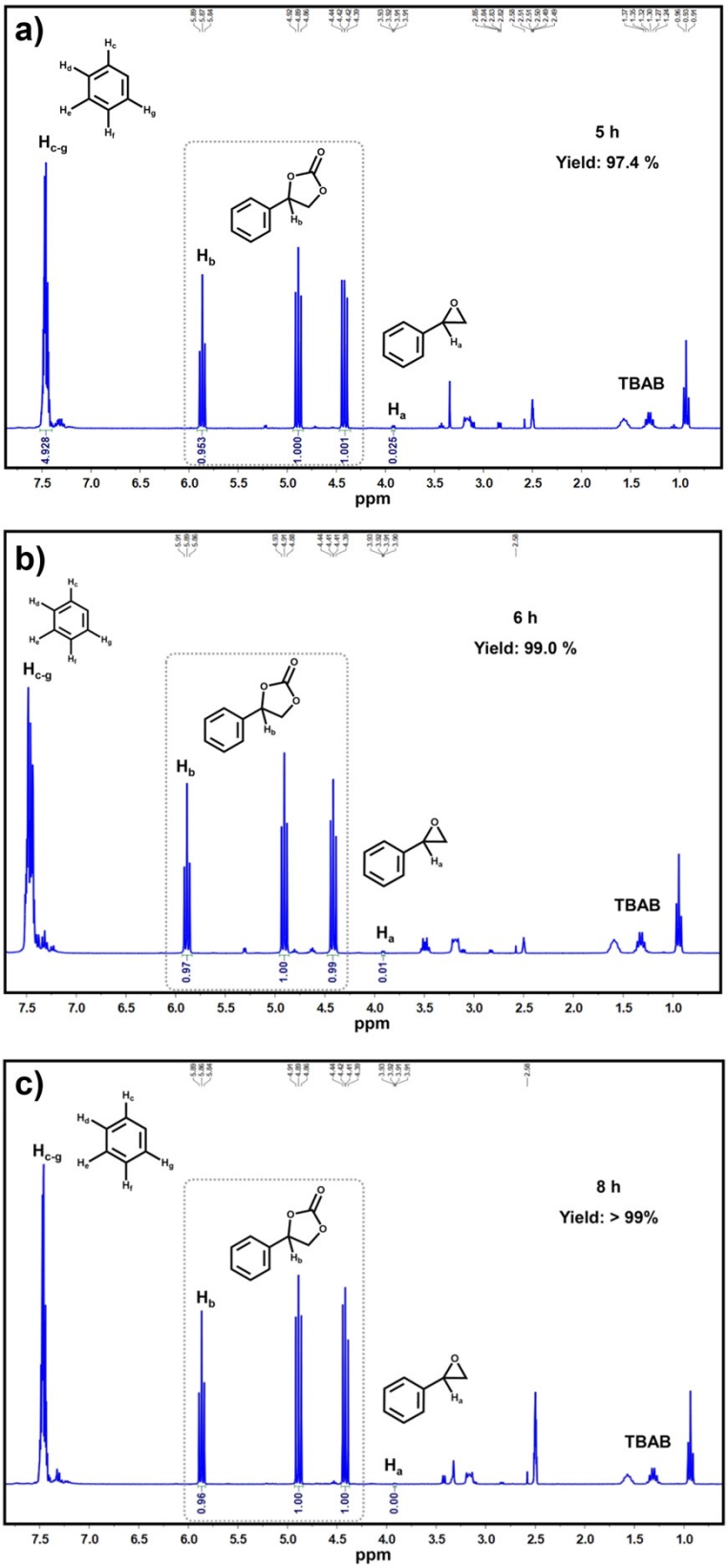

Fig. S21. ^{1}H NMR spectra of CO_2 conversion catalyzed by **JLU-MOF116** within a) 5 h, b) 6 h, and c) 8 h.

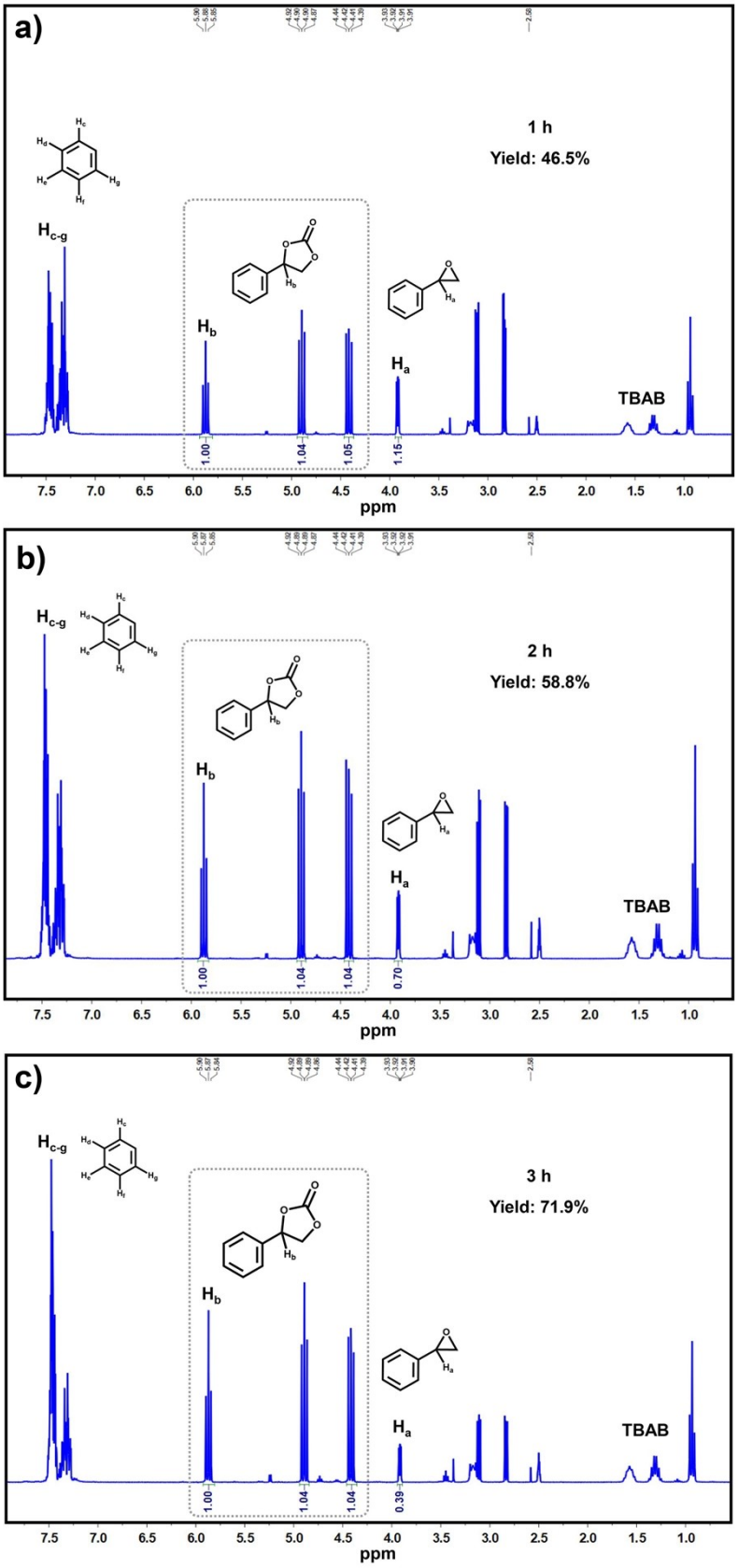

Fig. S22. ^{1}H NMR spectra of CO_2 conversion catalyzed by **JLU-MOF117** within a) 1 h, b) 2 h, and c) 3 h.

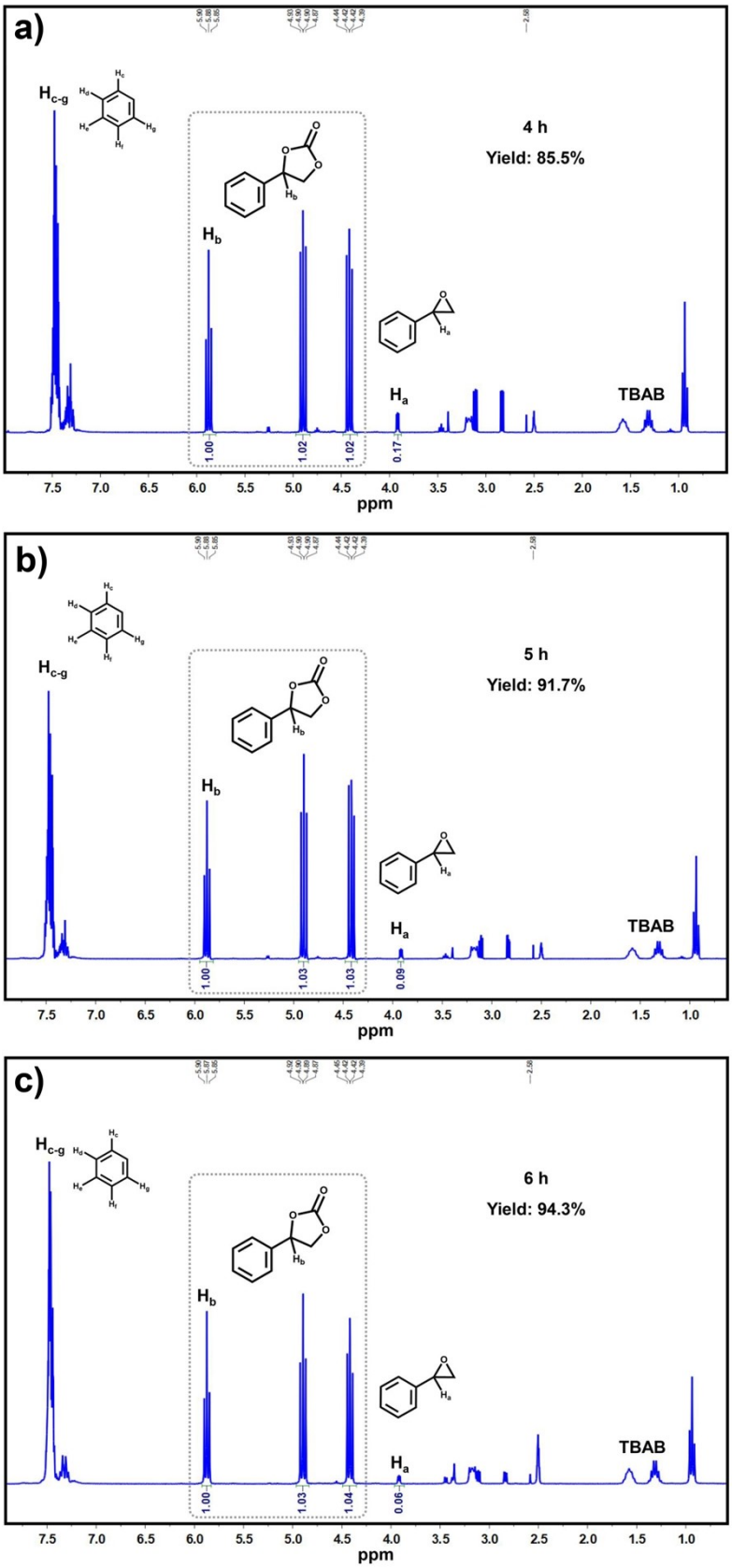

Fig. S23. ^{1}H NMR spectra of CO_2 conversion catalyzed by **JLU-MOF116** within a) 4 h, b) 5 h, and c) 6 h.

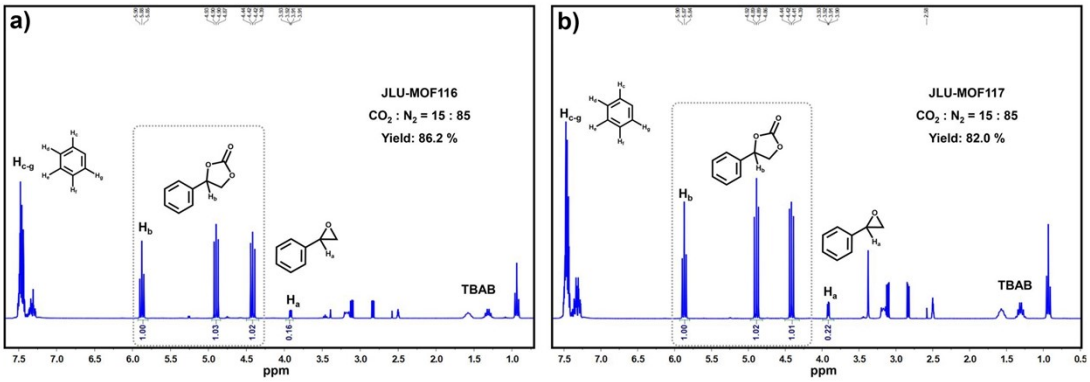

Fig. S24. CO_2 conversions by **JLU-MOF116** and **117** under 1 atm of CO_2 and N_2 mixed gases (CO_2/N_2, 15/85, v/v).

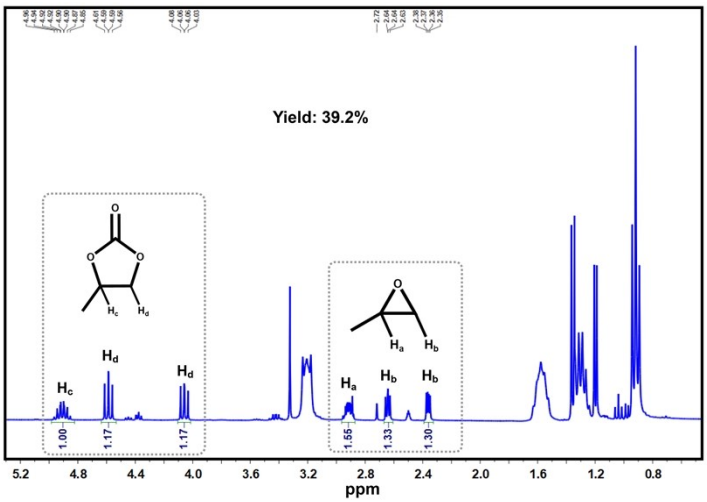

Fig. S25. ^{1}H NMR spectrum of CO_2 conversion with propylene oxide catalyzed by **JLU-MOF116**.

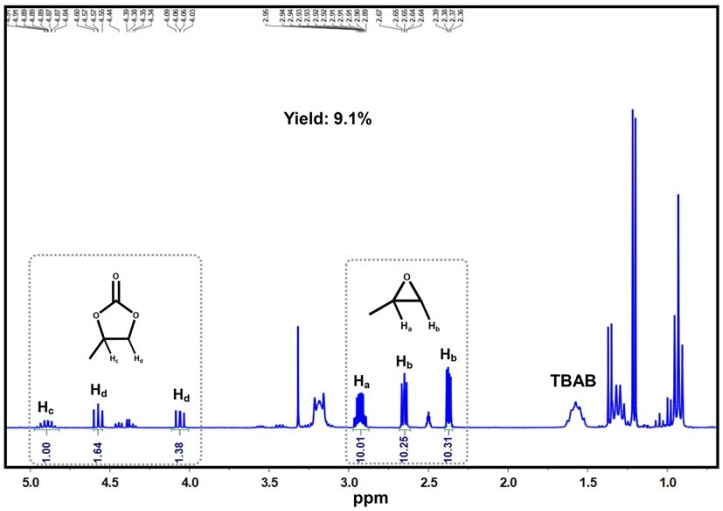

Fig. S26. ^{1}H NMR spectrum of CO_2 conversion with propylene oxide catalyzed by **JLU-MOF117**.

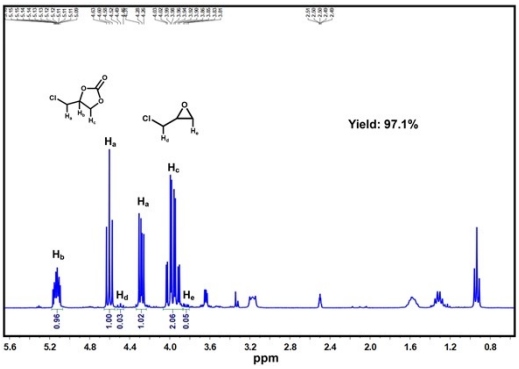

Fig. S27. ^{1}H NMR spectrum of CO_2 conversion with epoxy chloropropane catalyzed by **JLU-MOF116**.

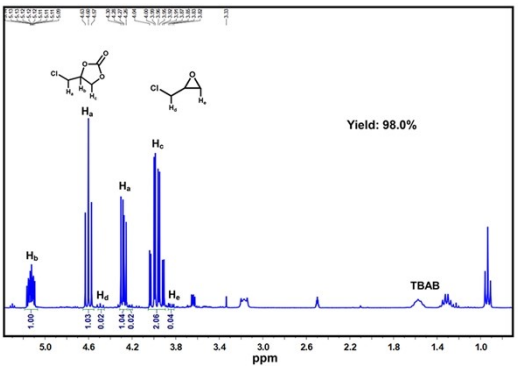

Fig. S28. ^{1}H NMR spectrum of CO_2 conversion with epoxy chloropropane catalyzed by **JLU-MOF117**.

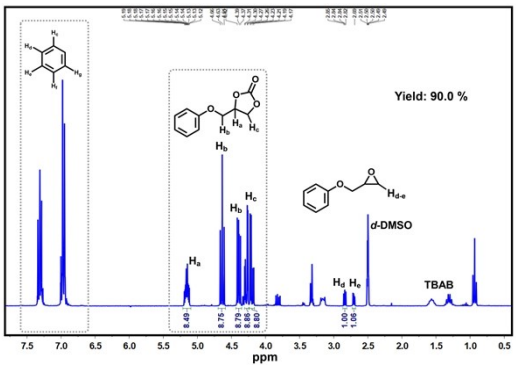

Fig. S29. ^{1}H NMR spectrum of CO_2 conversion with epoxypropyl phenyl ether catalyzed by **JLU-MOF116**.

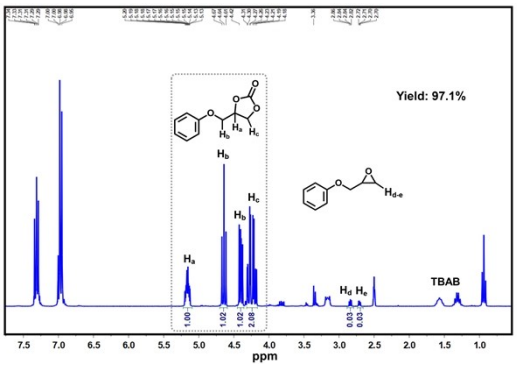

Fig. S30. ^{1}H NMR spectrum of CO_2 conversion with epoxypropyl phenyl ether catalyzed by **JLU-MOF117**.

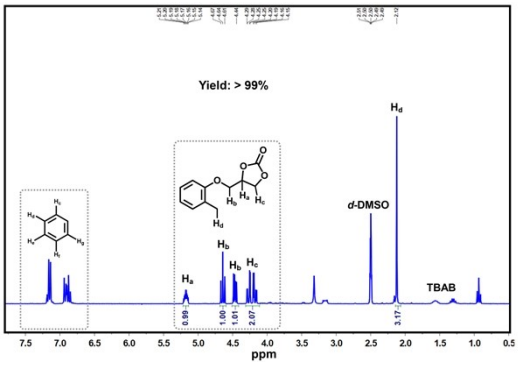

Fig. S31. ^{1}H NMR spectrum of CO_2 conversion with o-tolyl glycidyl ether catalyzed by **JLU-MOF116**.

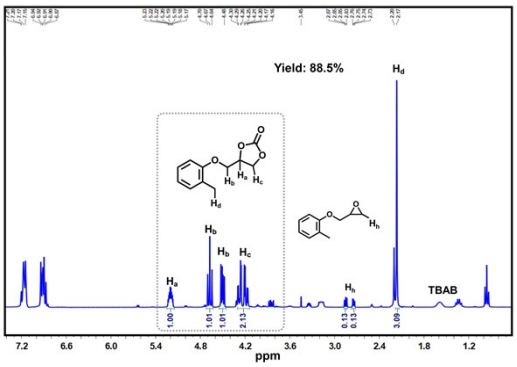

Fig. S32. ^{1}H NMR spectrum of CO_2 conversion with o-tolyl glycidyl ether catalyzed by **JLU-MOF117**.

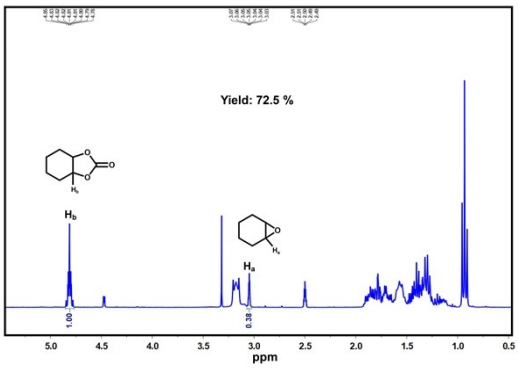

Fig. S33. ^{1}H NMR spectrum of CO_2 conversion with cyclohexene oxide catalyzed by **JLU-MOF116**.

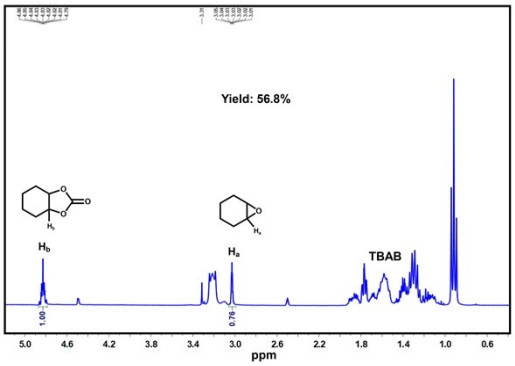

Fig. S34. ^{1}H NMR spectrum of CO_2 conversion with cyclohexene oxide catalyzed by **JLU-MOF117**.

Table S5. CO_2 cycloaddition catalytic efficiencies of **JLU-MOF116** and **117** in comparison with other MOF materials.

Substrate	Compound [a]	Time (h)	Yield (%)	TON	TOF (h^{-1})	Ref.
SO	Ce_2NDC_3	8	89	360	45.0	6
	MOF1	24	11	65	15.9	7
	Hf-NU-1000	56	100	400	7.1	8
	$In_2(OH)(btc)(Hbtc)_{0.4}(L)_{0.6}\cdot 3H_2O$	48	32	139	2.9	9
	$\{[Ba_2(BDPO)(H_2O)]\cdot DMA\}_n$	48	19.8	105	2.2	10
	$\{[Sr(BDPO)_{0.5}(H_2O)]\cdot 2H_2O\}_n$	48	18	21	0.4	11
	JLU-MOF117 [b]	6	94	940	156.7	This Work
	JLU-MOF116 [b]	5	97	647	129.4	This Work
ECH	Ce_2NDC_3	8	92	372	46.5	6
	MOF1	24	99	582	24.3	7
	FJI-H7(Cu)	60	67	333	5.5	12
	$\{[Ba_2(BDPO)(H_2O)]\cdot DMA\}_n$	48	90	180	3.8	10
	$[Cu(bpy)_2(EDS)]_n$	Not Mentioned	92	92		13
	JLU-MOF117 [b]	6	98	980	163.3	This Work
	JLU-MOF116 [b]	5	97	647	129.4	This Work

[a] Room temperature, 1 bar CO_2 pressure; [b] 60 ºC, 1 bar CO_2 pressure.

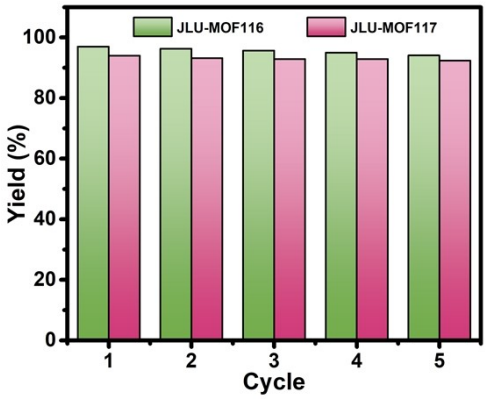

Fig. S35. The catalytic efficiencies of **JLU-MOF116** and **117** for CO_2 conversion within five cycles.

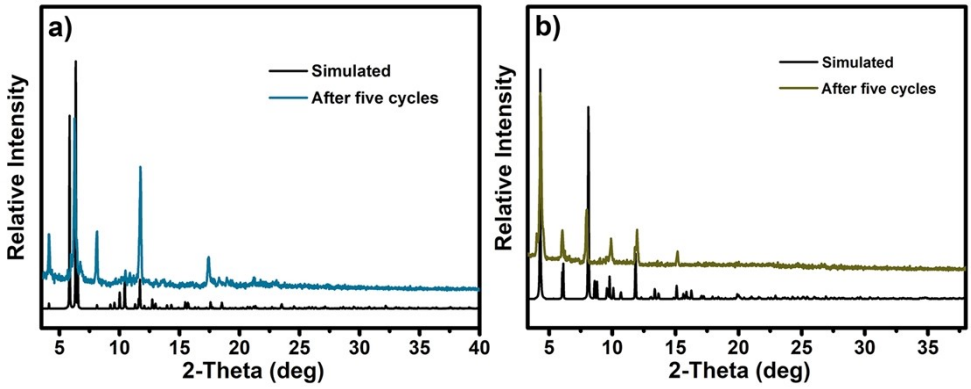

Fig. S36. PXRD patterns of a) **JLU-MOF116** and b) **JLU-MOF117** after five cycles of cycloadditions of styrene oxide with CO_2.

S5. Knoevenagel condensation reactions catalyzed by JLU-MOF116 and JLU-MOF117.

Table S6. The investigation of optimal reaction conditions of Knoevenagel condensation for **JLU-MOF116** and **JLU-MOF117.**

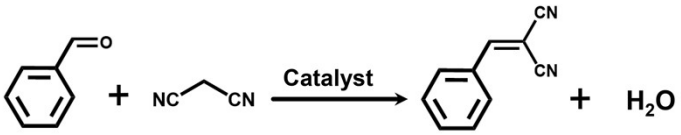

Entry	JLU-MOF116				Entry	JLU-MOF117			
	Cat. (mol%)	Temp. (°C)	Time (min)	Yield (%)		Cat. (mol%)	Temp. (°C)	Time (min)	Yield (%)
1	0.125	40	180	89	13	0.25	40	120	99
2	0.250	40	180	98	14	0.50	40	120	> 99
3	0.500	40	180	98	15	0.25	20	120	96
4	0.250	20	180	90	16	0.25	40	30	89
5	0.250	60	180	96	17	0.25	40	60	94
6	0.250	40	30	60	18	0.25	40	90	99
7	0.250	40	60	81	19	L2	40	90	24
8	0.250	40	90	93	20	None	40	90	21
9	0.250	40	120	95					
10	0.250	40	150	97					
11	L1	40	120	3					
12	None	40	120	30					

Reaction conditions: Benzaldehyde (2 mmol), malononitrile (3 mmol), EtOH (4 mL).

Malononitrile (3 mmol) and benzaldehyde (2 mmol) were chosen as substrates to investigate optimal conditions. The amount of MOF catalysts was investigated initially. The reactions catalyzed by 0.25 mol% and 0.5 mol% **JLU-MOF116** resulted in a 98% yield, while the reduction of **JLU-MOF116** to 0.125 mol% led to a negligible decline to an 89% yield (Table S6, Entry 1-3). Thereby, the amount of **JLU-MOF116** was determined as 0.25 mol%. **JLU-MOF117** was also determined as 0.25 mol% with a 99% yield for ease of comparison. The optimal reaction time and temperature were determined by time-varying kinetic curves under different temperatures to be 120 min/40 °C for **JLU-MOF116** and 90 min/40 °C for **JLU-MOF117**, respectively (Table S6, Entry 6-10 and 16-18, and Figure S42).

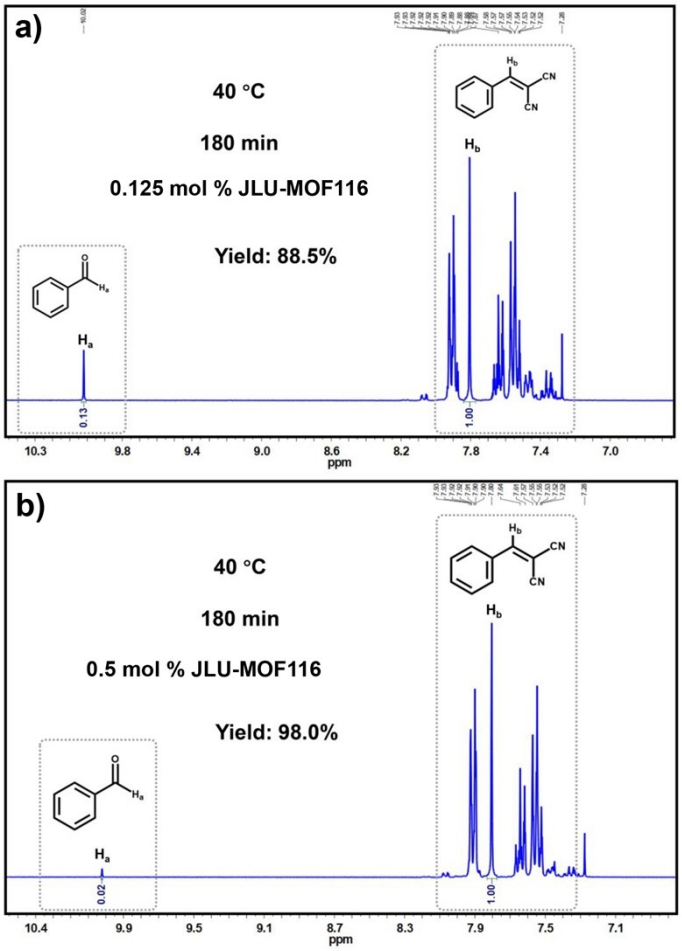

Fig. S37. ^{1}H NMR spectra of Knoevenagel condensation reactions catalyzed by a) 0.125 mol% and b) 0.5 mol% **JLU-MOF116**.

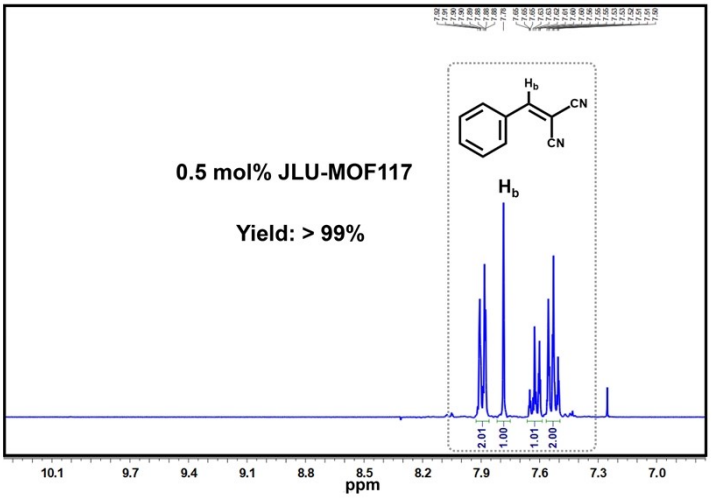

Fig. S38. ^{1}H NMR spectra of Knoevenagel condensation reactions catalyzed by 0.5 mol% **JLU-MOF117**.

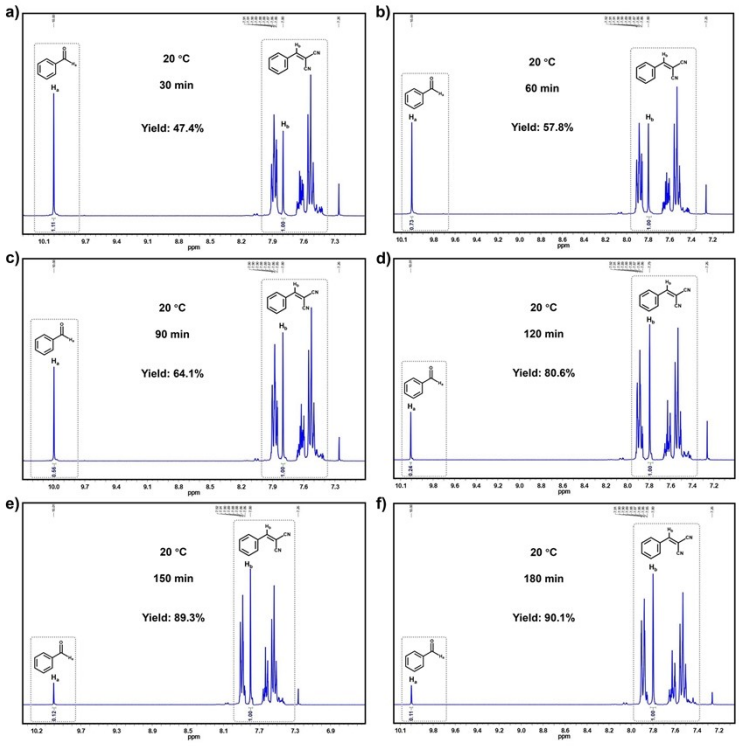

Fig. S39. ^{1}H NMR of Knoevenagel condensation reactions catalyzed by **JLU-MOF116** at 20 °C within a) 30, b) 60, c) 90, d) 120, e) 150, and f) 180 min.

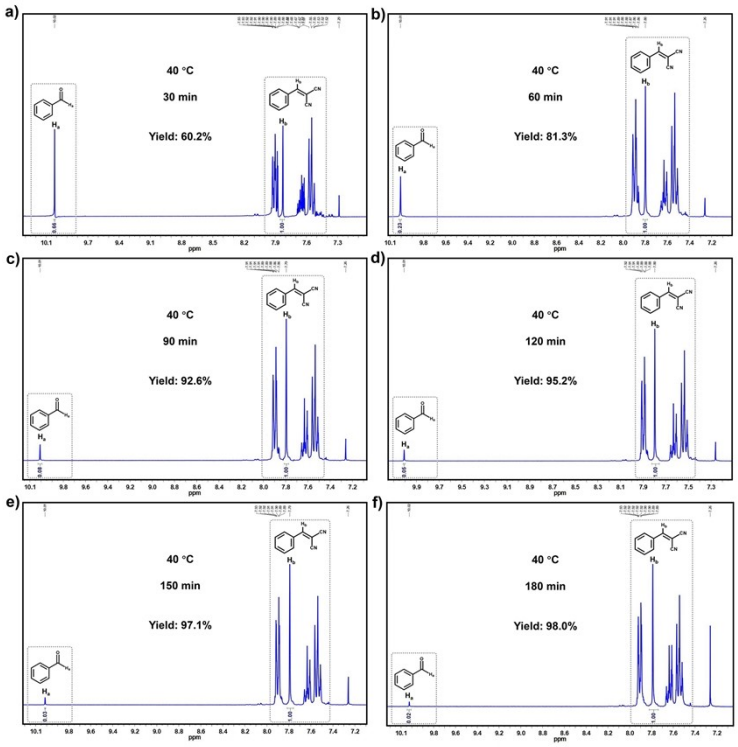

Fig. S40. ^{1}H NMR of Knoevenagel condensation reactions catalyzed by **JLU-MOF116** at 40 °C within a) 30, b) 60, c) 90, d) 120, e) 150, and f) 180 min.

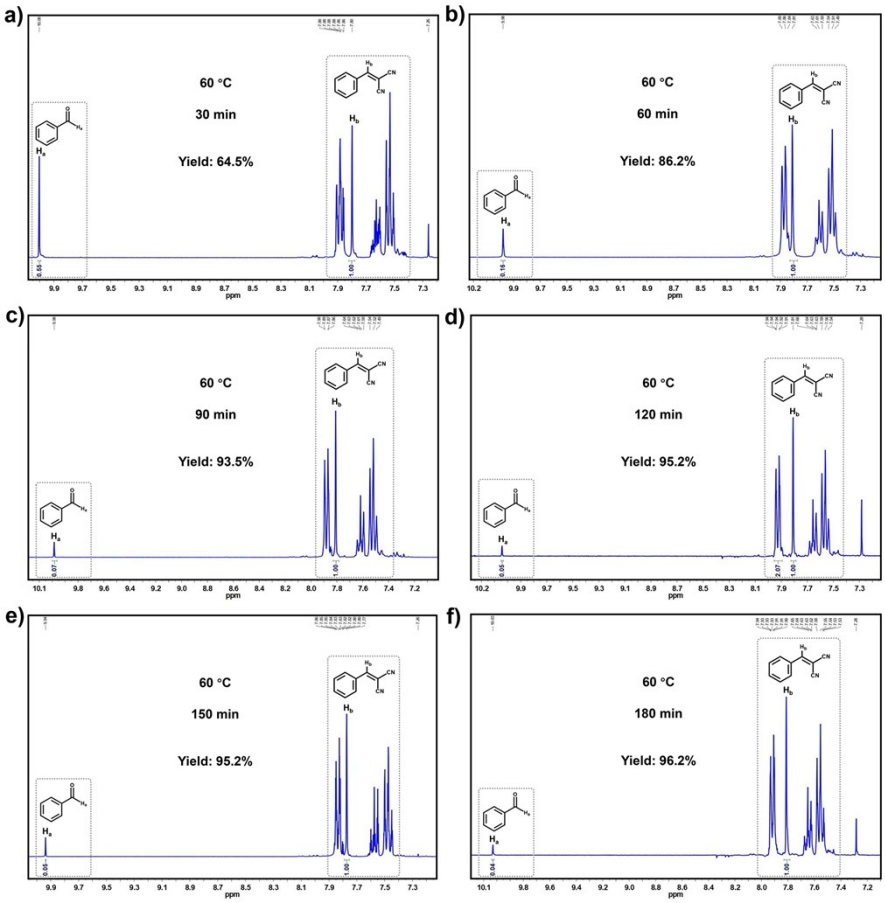

Fig. S41. ^{1}H NMR of Knoevenagel condensation reactions catalyzed by **JLU-MOF116** at 60 °C within a) 30, b) 60, c) 90, d) 120, e) 150, and f) 180 min.

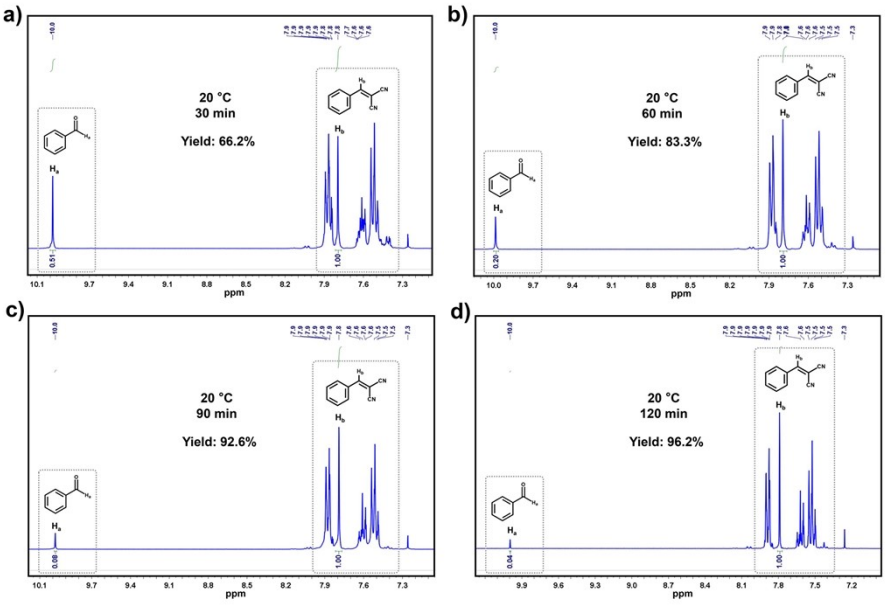

Fig. S42. ^{1}H NMR of Knoevenagel condensation reactions catalyzed by **JLU-MOF117** at 20 °C within a) 30, b) 60, c) 90, and d) 120 min.

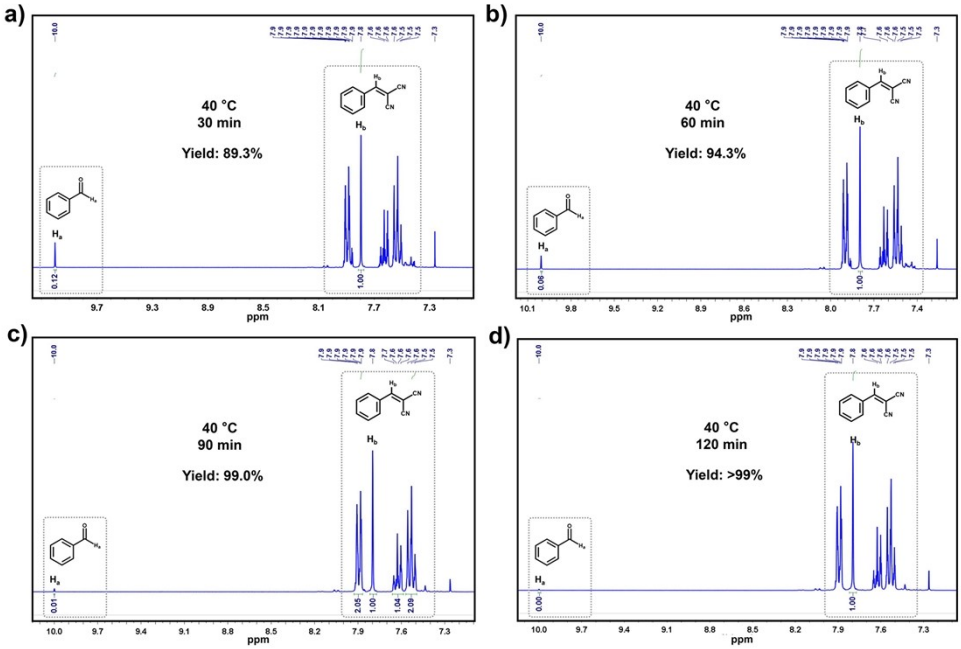

Fig. S43. ^{1}H NMR of Knoevenagel condensation reactions catalyzed by **JLU-MOF117** at 40 °C within a) 30, b) 60, c) 90, and d) 120 min.

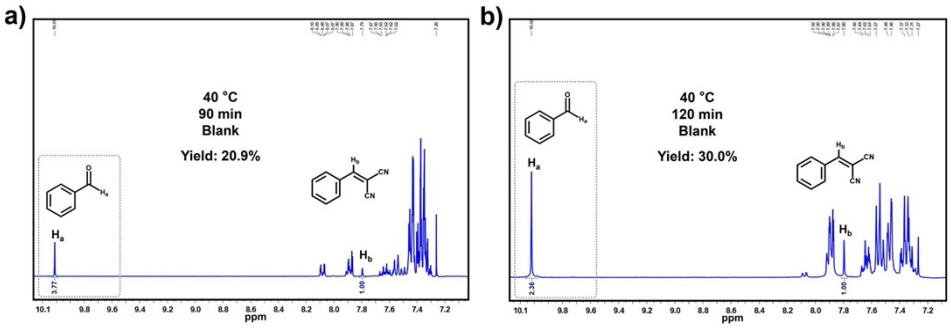

Fig. S44. Knoevenagel condensation reactions without catalyst within a) 90 min and b) 120 min.

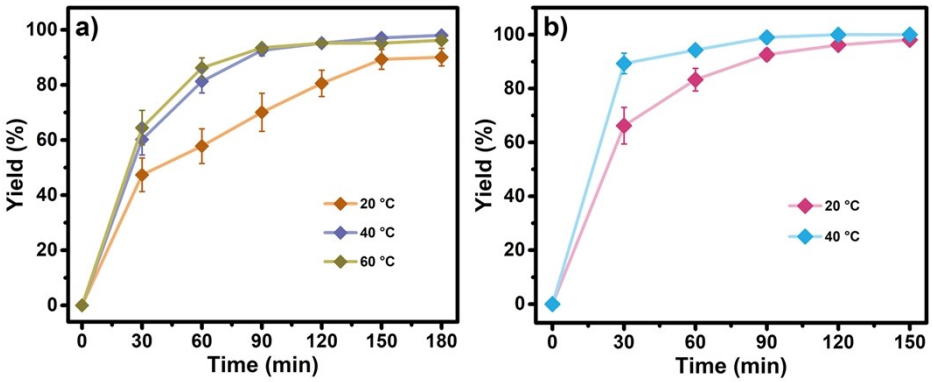

Fig. S45. Time-varying kinetic curves of a) **JLU-MOF116** and b) **JLU-MOF117** for Knoevenagel condensation.

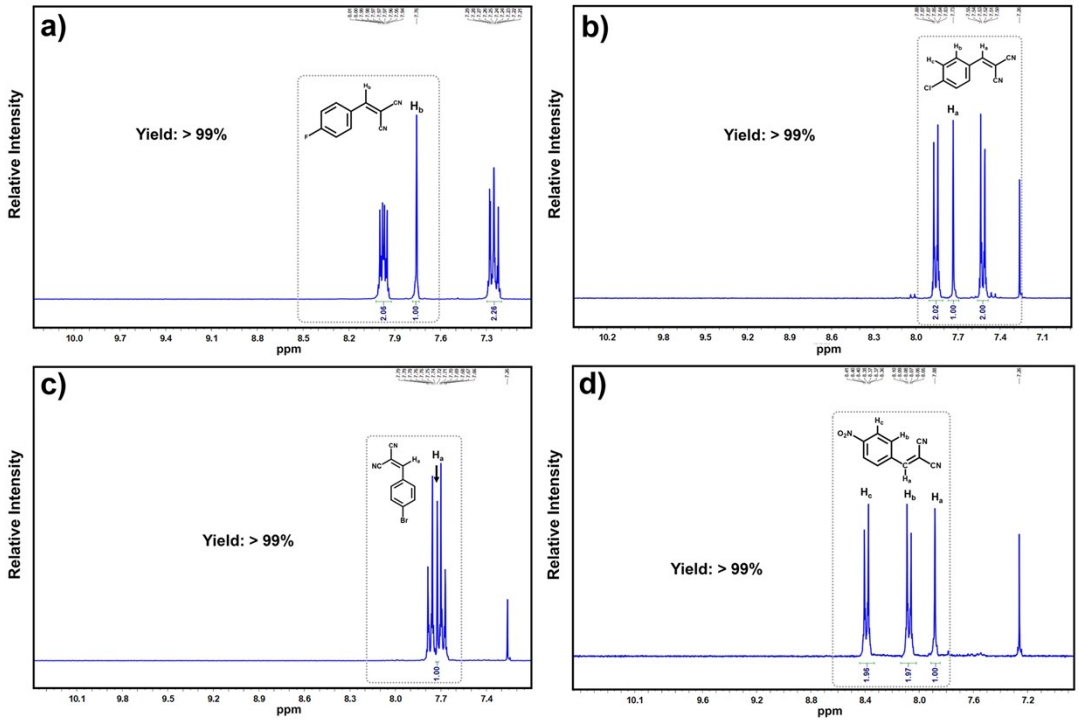

Fig. S46. ^{1}H NMR spectra of the Knoevenagel condensation by **JLU-MOF116** with a) 4-fluorobenzaldehyde, b) 4-chlorobenzaldehyde, c) 4-bromobenzaldehyde, and d) 4-nitrobenzaldehyde as reactants.

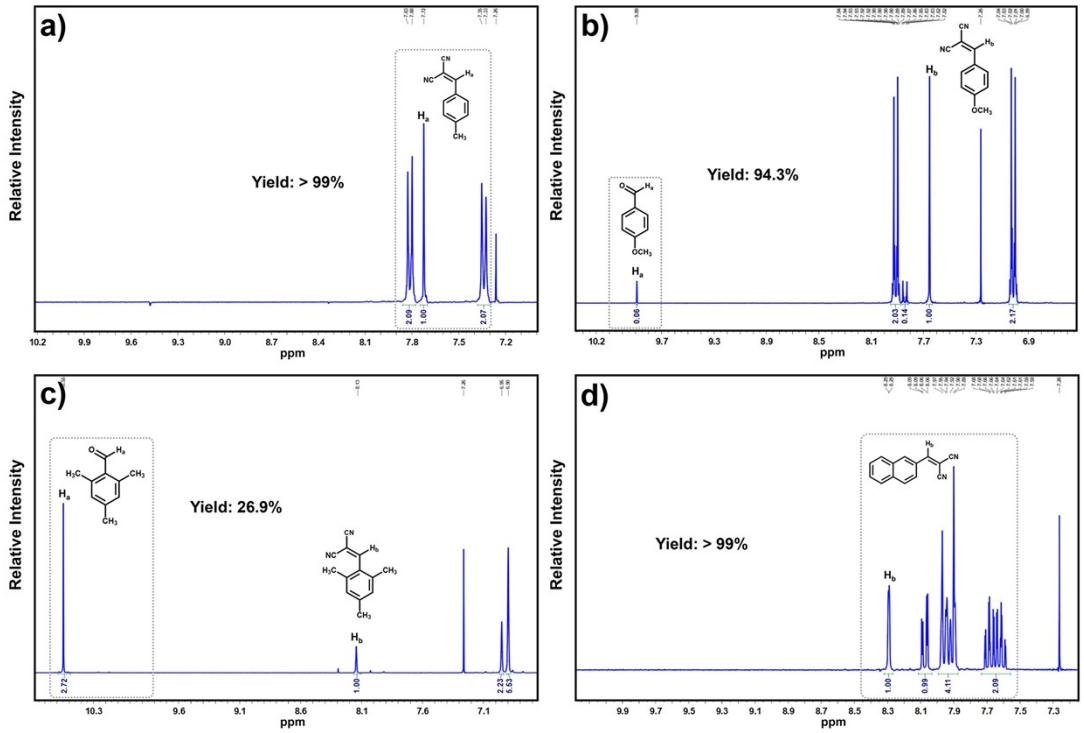

Fig. S47. ^{1}H NMR spectra of the Knoevenagel condensation by **JLU-MOF116** with a) 4-methyl benzaldehyde, b) 4-anisaldehyde, c) 2,4,6-trimethylbenzaldehyde, and d) 2-naphthaldehyde as reactants.

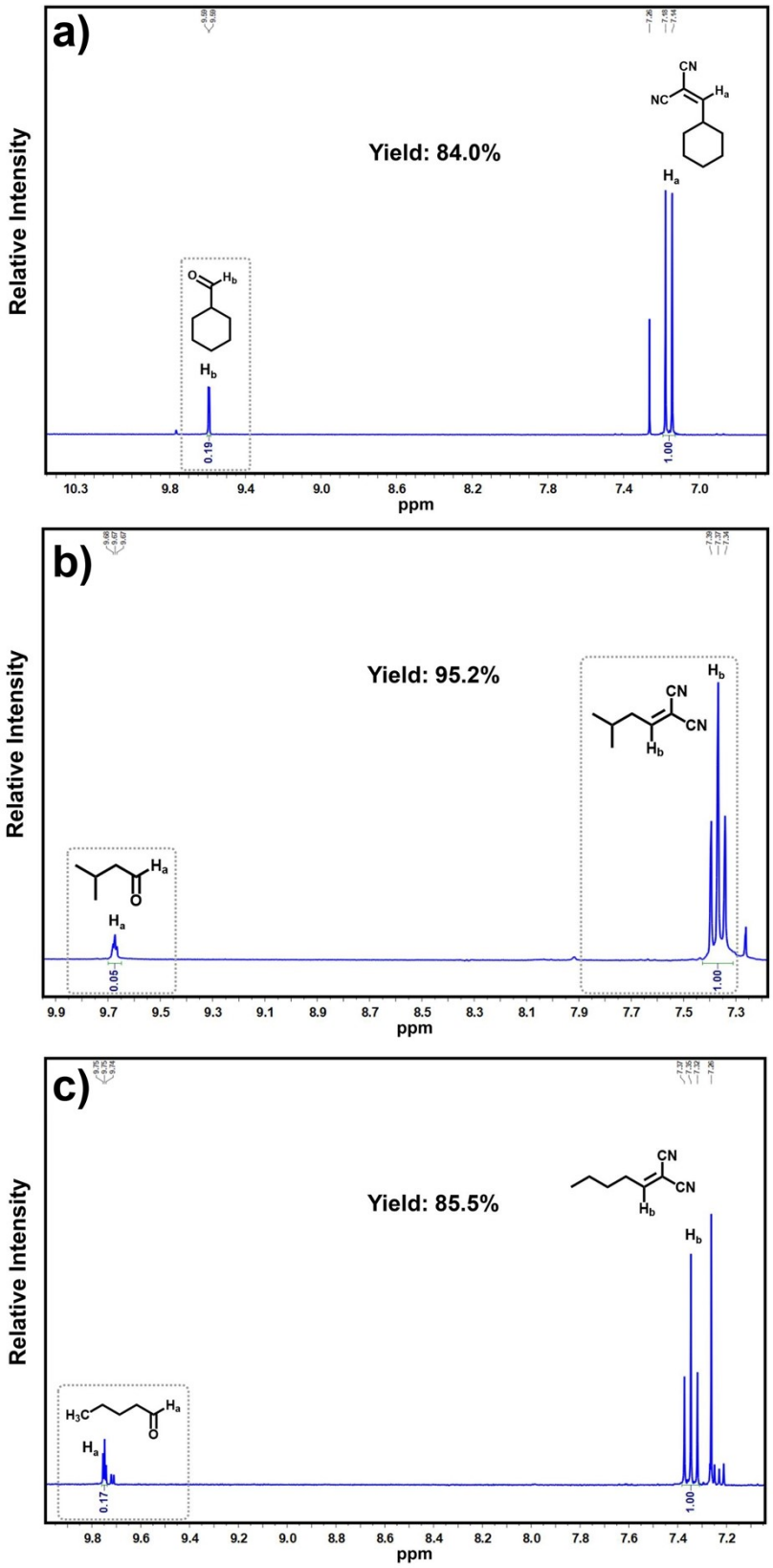

Fig. S48. ^{1}H NMR spectra of the Knoevenagel condensation by **JLU-MOF116** with a) cyclohexanecarboxaldehyde, b) pentanal, and c) isovaleraldehyde as reactants.

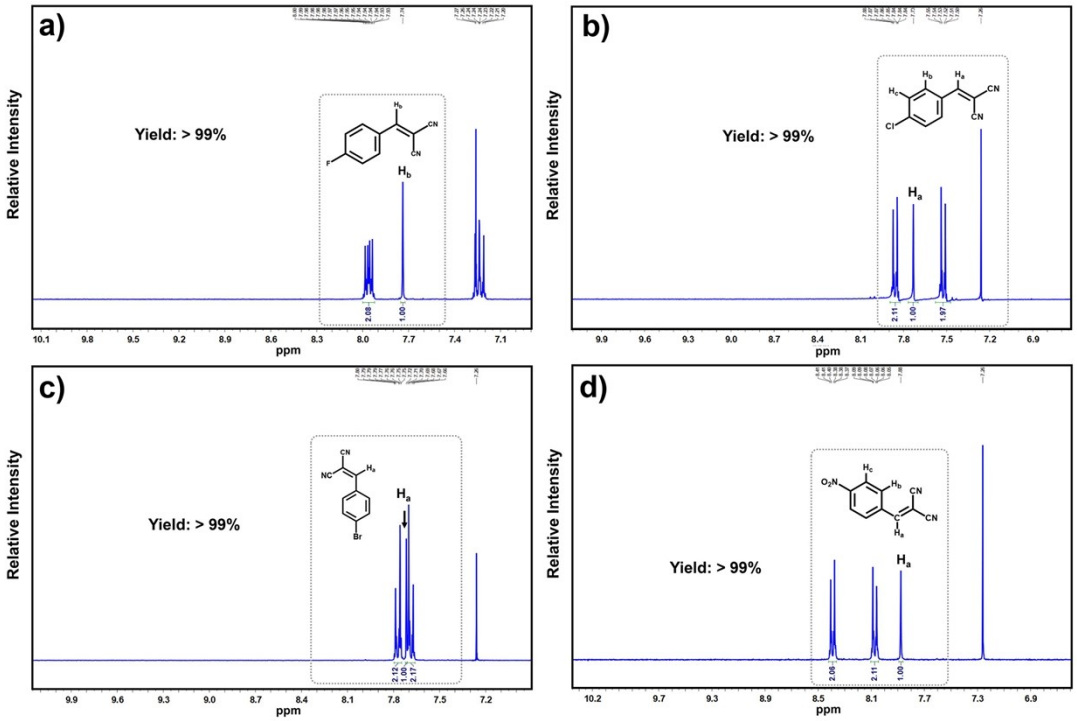

Fig. S49. ^{1}H NMR spectra of the Knoevenagel condensation by **JLU-MOF117** with a) 4-fluorobenzaldehyde, b) 4-chlorobenzaldehyde, c) 4-bromobenzaldehyde, and d) 4-nitrobenzaldehyde as reactants.

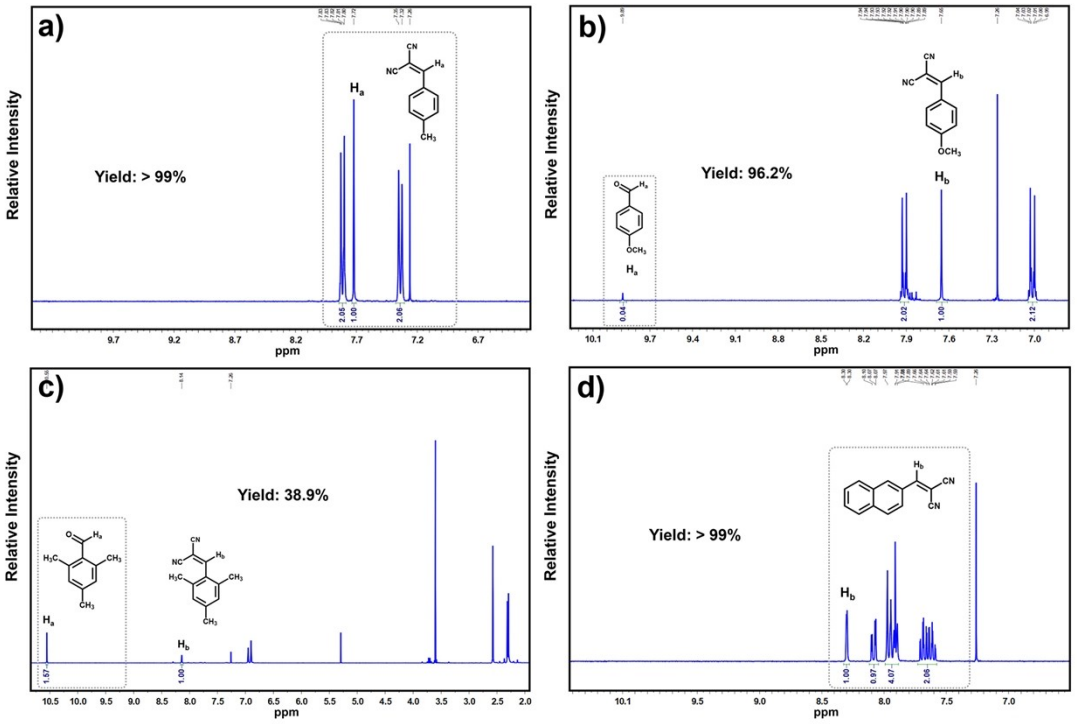

Fig. S50. ^{1}H NMR spectra of the Knoevenagel condensation by **JLU-MOF117** with a) 4-methyl benzaldehyde, b) 4-anisaldehyde, c) 2,4,6-trimethylbenzaldehyde, and d) 2-naphthaldehyde as reactants.

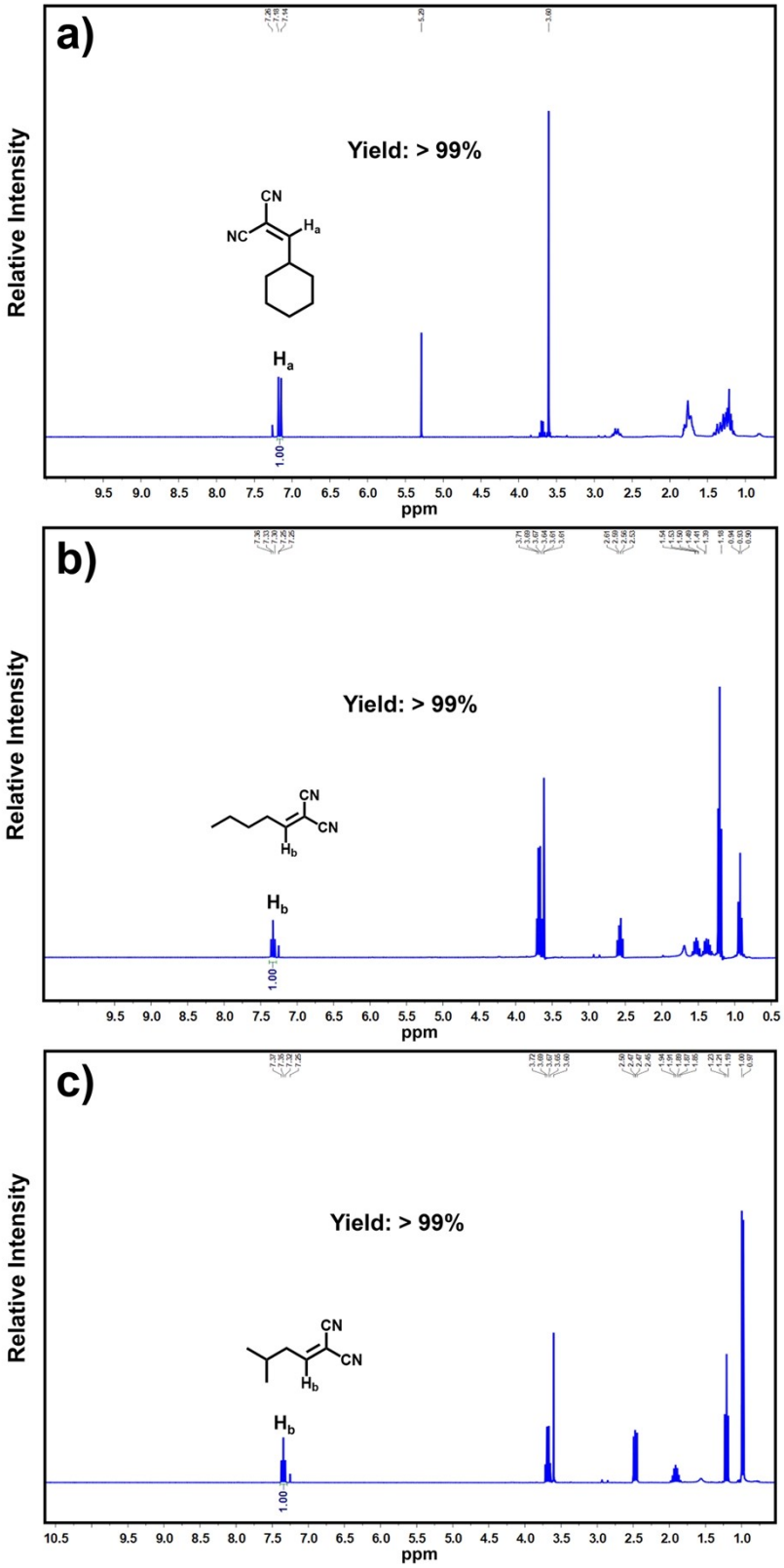

Fig. S51. ^{1}H NMR spectra of the Knoevenagel condensation by **JLU-MOF117** with a) cyclohexanecarboxaldehyde, b) pentanal, and c) isovaleraldehyde as reactants.

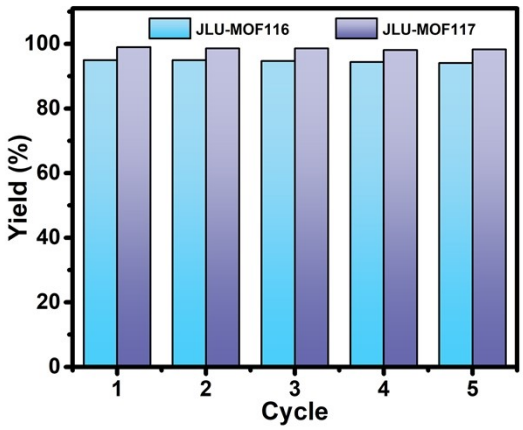

Fig. S52. The catalytic performances of **JLU-MOF116** and **117** for Knoevenagel condensation within five cycles.

Table S7. Knoevenagel condensation catalytic efficiencies of **JLU-MOF116** and **117** in comparison with other MOF materials.

Compound	Cat. (mol%)	Solvent	Temp. (°C) & Time (h)	Yield (%)	TON	TOF (min^{-1})	Ref.
JLU-MOF117	0.25	Ethanol	40 °C/1.5 h	99	396	4.40	This work
JLU-MOF116	0.25	Ethanol	40 °C/2 h	95	380	3.17	This work
NUC-21	0.3	Solvent free	70 °C/1 h	97	323	5.38	14
$[Co_2(bptc)(H_2O)_2]\cdot5DMA$	2	Solvent free	60 °C/6 h	> 99	50	0.14	15
MOF3	0.25	DMF	RT/6 h	97	388	1.08	16
NUC-25	0.4	Solvent free	80 °C/24 h	99	248	0.17	17
$[Zn(\kappa N\text{-}H_3L)(H_2O)_3]\cdot3H_2O$	3	THF	50 °C/4 h	94	31	0.13	18
NUC-38Yb	0.3	Ethanol	45 °C/24 h	96	1280	0.89	19
NUC-28	0.3	Ethanol	45 °C/24 h	96	320	0.22	20
UiO-66-NH-RNH_2	1	Toluene	RT/2 h	97	97	0.81	21
$[Cu_2(\mu\text{-}H_3ddba)_2(phen)_2]$	2	H_2O	25 °C/1 h	> 99	50	0.83	22

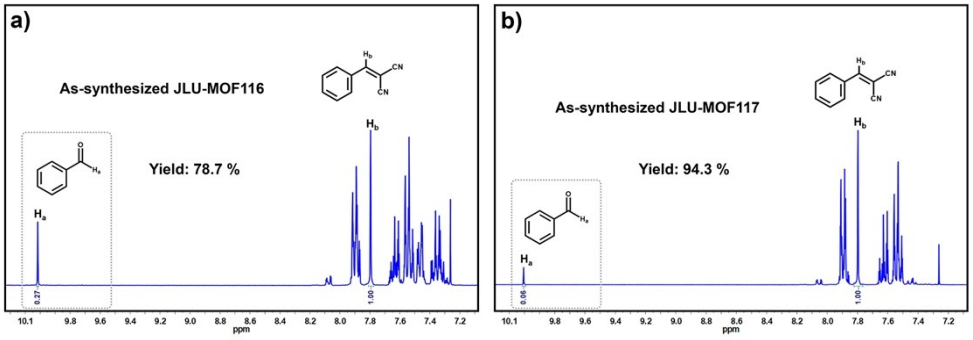

Fig. S53. The Knoevenagel condensation reactions by 0.25 mol as-synthesized **JLU-MOF116** and **JLU-MOF117**, respectively.

Reference

1. J. Y. Qiao, B. R. Zhang, X. Y. Yu, X. Q. Zou, X. Y. Liu, L. R. Zhang and Y. L. Liu, *Inorg. Chem.*, 2022, **61***,* 3708–3715*.*

2. Y. F. Zhang, Z. H. Zhang, L. Ritter, H. Fang, Q. Wang, B. Space. Y. B. Zhang, D. X. Xue and J. F. Bai, *J. Am. Chem. Soc.*, 2021, **143**, 12202–12211.

3. H. Jiang, J. T. Jia, A. Shkurenko, Z. J. Chen, K. Adil, Y. Belmabkhout, L. J. Weselinski, A. H. Assen, D. X. Xue, M. O'Keeffe and M. Eddaoudi, *J. Am. Chem. Soc.*, 2018, **140**, 8858–8867.

4. B. S. Zheng, J. F. Bai, J. G. Duan, L. Wojtas and M. J. Zaworotko, *J. Am. Chem. Soc.*, 2011, **133**, 748–751.

5. R. Grünker, V. Bon, P. Müller, U. Stoeck, S. Krause, U. Mueller, I. Senkovska and S. Kaskel, *Chem. Commun.*, 2014, **50**, 3450–3452.

6. S. K. Das, S. Chatterjee, S. Bhunia, A. Mondal, P. Mitra, V. Kumari, A. Pradhan and A. Bhaumik, *Dalton Trans.*, 2017, **46**, 13783–13792.

7. G. Chakraborty, P. Das and S. K. Mandal, *Inorg. Chem.*, 2021, **60**, 5071–5080.

8. H. Beyzavi, R. C. Klet, S. Tussupbayev, J. Borycz, N. A. Vermeulen, C. J. Cramer, J. F. Stoddart, J. T. Hupp and O. K. Farha, *J. Am. Chem. Soc.*, 2014, **136**, 15861–15864.

9. L. Liu, S. M. Wang, Z. B. Han, M. L. Ding, D. Q. Yuan and H. L. Jiang, *Inorg. Chem.*, 2016, **55**, 3558–3565.

10. X. Y. Li, L. N. Ma, Y. Liu, L. Hou, Y. Y. Wang and Z. H. Zhu, *ACS Appl. Mater. Interfaces*, 2018, **10**, 10965–10973.

11. X. Y. Li, Y. Z. Li, Y. Yang, L. Hou, Y. Y. Wang and Z. H. Zhu, *Chem. Commun.*, 2017, **53**, 12970–12973.

12. J. Zheng, M. Y. Wu, F. L. Jiang, W. P. Su and M. C. Hong, *Chem. Sci.*, 2015, **6**, 3466–3470.

13. G. Y. Zhang, G. F. Wei, Z. P. Liu, S. R. J. Oliver and H. H. Fei, *Chem. Mater.*, 2016, **28**, 6276–6281.

14. H. T. Chen, L. M. Fan and X. T. Zhang, ACS Appl. Mater. Interfaces, 2020, 12, 54884–54892.

15. J. B. Deng, X. Wang, Z. Q. Ni and F. Zhu, *Arab. J. Chem.*, 2020, **13**, 7482–7489.

16. Y. Y. Zhang, Q. Liu, L. Y. Zhang, Y. M. Bao, J. Y. Tan, N. Zhang, J. Y. Zhang and Z. J. Liu, *Dalton Trans.*, 2021, **50**, 647–659.

17. H. Chen, T. Hu, L. Fan and X. Zhang, *Inorg. Chem.*, 2021, **60**, 1028–1036.

18. A. Karmakar, A. Paul, K. T. Mahmudov, M. F. C. Guedes da Silva and A. J. L. Pombeiro, *New J. Chem.*, 2016, **40**, 1535–1546.

19. T. Zhang, H. Chen, S. Liu, H. Lv, X. Zhang and Q. Li, *ACS Catal.*, 2021, **11**, 14916–14925.

20. T. Zhang, Z. Zhang, H. Chen, X. Zhang and Q. Li, *Cryst. Growth Des.*, 2021, **22**, 304–312.

21. Y. Luan, Y. Qi, H. Gao, R. S. Andriamitantsoa, N. Zheng and G. Wang, *J. Mater. Chem. A*, 2015, **3**, 17320–17331.

22. H. R. Zhang, J. Z. Gu, M. V. Kirillova and A. M. Kirillov, *Inorg. Chem. Front.*, 2021, **8**, 4209–4221.